ELSEVIER

Contents lists available at ScienceDirect

Journal of Non-Crystalline Solids

journal homepage: www.elsevier.com/locate/jnoncrysol





Compositional dependence of crystallization and chemical durability in alkali aluminoborosilicate glasses

Ambar Deshkar^a, Benjamin Parruzot^b, Randall E. Youngman^c, Ozgur Gulbiten^c, John D. Vienna^b, Ashutosh Goel^{a,*}

- a Department of Materials Science and Engineering, Rutgers, The State University of New Jersey, Piscataway, NJ 08854-8065, United States
- ^b Pacific Northwest National Laboratory, Richland, WA 99352, United States
- ^c Science and Technology Division, Corning Incorporated, Corning, NY 14831, United States

ARTICLE INFO

Keywords: Glass Crystallization Chemical durability Nuclear waste

ABSTRACT

This study aims to understand the impact of composition on crystallization and chemical durability in alkali aluminoborosilicate based model nuclear waste glasses designed in the peralkaline, metaluminous and peraluminous regimes. The glasses have been thermally treated using the canister centerline cooling (CCC) schedule. The chemical durability of both parent and CCC-treated glasses has been assessed by product consistency test (PCT-B) for 120 days. The peraluminous glasses exhibit the highest dissolution rates, followed by peralkaline and metaluminous glasses. In general, increasing B_2O_3 content in glasses tends to suppress nepheline formation, thus, decreasing the negative impact of nepheline on durability of the final waste form. However, higher B_2O_3 content itself may result in detrimental impact on the durability of the final waste form. The thermal history has been shown to have a significant impact on the durability of the glasses.

1. Introduction

Nearly five decades of plutonium production in the support of U.S. defense programs has generated ~56 million gallons of radioactive and chemical wastes at the U.S. Department of Energy's (DOE) Hanford Site in Washington state [1]. The waste is currently stored inside 177 underground tanks, wherein the contents of these tanks include a complex sludge, salt cake, and supernate mixed radioactive waste [1]. Bechtel National Inc. is constructing the Hanford Tank Waste Treatment and Immobilization Plant to vitrify the high-level waste (HLW) and low-activity waste (LAW) fractions into alkali-aluminoborosilicate-based glassy waste forms [2-4]. The waste-to-glass conversion will be achieved by mixing glass-forming precursors like SiO2 and H3BO3 (as a source of B2O3) in the waste feed followed by melting the mixture in Joule heated ceramic melters (JHCM), and subsequently pouring the melt into stainless steel canisters to cool and solidify [5-7]. While SiO2 has been chosen as the primary glass network former, B₂O₃ has been chosen as a flux to lower the melting temperature of the batch (waste feed + glass-forming oxides), to enable the vitrification of waste at ~ 1150 °C. As per the current strategy for nuclear waste disposal, the steel canisters containing the vitrified HLW glasses will be transported to a geological repository, while

the LAW steel containers will be managed at an on-site integrated disposal facility (IDF).

When in the geological repository, it is expected that the intrusion of groundwater into and through the repository will be the most likely mechanism by which radionuclides will be removed from the nuclear waste glass once the canister undergoes its eventual degradation (after thousands of years) [8]. Due to this reason, nuclear waste glasses are formulated to maintain their chemical stability (when in contact with water) over geological time scales.

One of the significant impediments towards the chemical durability of some nuclear waste glasses is the crystallization of nepheline (NaAl-SiO₄) that occurs during cooling of the glass melt in a steel canister in compositions containing high concentrations of Na₂O and Al₂O₃ [9]. Since one mole of nepheline removes roughly three moles of network forming oxides (1 Al₂O₃ and 2 SiO₂) from the glassy matrix [10], this creates a shift in the residual glass composition, thus negatively affecting the chemical durability of the waste form [11] [12]. In the past three decades, intensive research efforts have been made at the U.S. DOE national laboratories and universities aimed at (i) understanding the underlying chemical, structural and thermodynamic drivers controlling the crystallization of nepheline in these glasses [6, 10, 12-23], and (ii)

E-mail address: ag1179@soe.rutgers.edu (A. Goel).

^{*} Corresponding author.

developing empirical models to predict nepheline crystallization in nuclear waste glasses [3, 24-29]. The overarching goal of the effort is to formulate glass compositions with enhanced waste loadings and minimal tendency towards nepheline crystallization.

The most recent models in the pursuit of predicting nepheline crystallization in nuclear waste glasses are the submixture model (SM) [3], and machine-learning based "difference based on correlation" (DC) descriptor [25, 29]. The SM predicts the propensity and concentration (vol.%) of nepheline crystallization in an HLW glass composition by plotting the composition on a pseudo-ternary phase diagram comprising alkali and alkaline earth oxides (Na2O, Li2O, K2O, MgO, CaO) as one pseudo-component, Al₂O₃ and Fe₂O₃ as the second pseudo-component, and SiO₂, B₂O₃, and P₂O₅ as the third pseudo-component [3, 30]. The model takes into account previously known effects, such as the suppressing effect of B₂O₃ on nepheline crystallization (especially when replaced for Al₂O₃) [16] and an opposite effect of Li₂O [3]. Although this model has proved to be better at predicting the probability of nepheline formation than its predecessors [3], it lacks sufficient experimental data for predicting nepheline crystallization over a broader compositional range [31]. Similarly, the DC descriptor model uses an extended dataset of nuclear waste glasses from the SM and employs a data-driven approach to create a mass fraction difference between oxides that promote nepheline crystallization (for example Al₂O₃, Na₂O, Li₂O) and those that suppress nepheline crystallization (for example, B2O3). The data-driven model has been found to predict nepheline crystallization with an accuracy of \sim 92% [25], a significant improvement as compared to previous models. Based on 747 total reported glass compositions, its fit has a lower misclassification rate of 8.3% - 62 glasses misclassified out of the 747 [3]. However, it also discusses the existence of an overlapping region in the compositional space where similar compositions exhibit different crystallization behavior, thus reducing the accuracy of the model. Therefore, in order to improve the accuracy of predictive models, it is necessary to collect more experimental data that explores the compositional effects and interactions of the key components in waste glass compositions using a more fundamental approach.

Further, it is crucial to account for the impact of thermal history on the chemical durability of borosilicate glasses to gain an in-depth understanding of the factors affecting the long-term performance of the nuclear waste glasses. The literature on this subject reveals that the short-to-medium range structure of borosilicate glasses is highly sensitive to the change in their thermal history [32–36], which in return affects their dissolution kinetics [37, 38]. It is obvious that the molecular structure of nuclear waste glasses (inside the steel canister) will be altered as a function of cooling profiles (from melt–to–glass). However, the impact of change in the structure (as a function of thermal history) on the chemical durability of these glasses is yet to be determined.

With the above-mentioned perspective, the present study is focused on understanding the compositional dependence of nepheline crystallization in the model HLW glasses designed in Li₂O-Na₂O-Al₂O₃-B₂O₃-SiO₂ system, followed by its subsequent impact on the chemical durability of the final waste form. The glass compositions investigated in the present study are the simplified derivatives of the baseline glass investigated by Kroll et al. [39], that reports about the unexplainable non-linear trends of nepheline formation in the glasses as a function of the linear combinations of component concentrations. Since varying the Li⁺:Na⁺ ratio in the glasses has been shown to have minimal impact on their propensity towards aluminosilicate phase crystallization (and resulting chemical durability) [18, 40, 41], and while increasing the concentration of Si-O-B, Si-O-Si, and Al-O-P linkages (over Si-O-Al linkages) has been shown to suppress nepheline crystallization [15, 42, 43], the emphasis in the present investigation is understanding the impact of mixed network former effects on the crystallization tendency (and chemical durability) of alkali aluminoborosilicate glasses over a broad composition space. Accordingly, glasses with varying B₂O₃:SiO₂ have been designed in peralkaline ([Li+Na]/[Al] > 1), metaluminous (Li+Na]/[Al] = 1), and

peraluminous (Li+Na]/[Al] < 1) regimes due to the known dependence of aluminum and boron speciation on the alkali–to–aluminum ratio [44–47]. Further, glasses with varying $B_2O_3{:}Al_2O_3$ and $Al_2O_3{:}SiO_2$ ratios (on molar basis) have been designed and studied in the peralkaline region of the investigated glass system.

The glasses in this study have been subjected to canister centerline cooling (CCC) treatment [3, 31], which is an emulation of the thermal profile that is expected at the center of an HLW melt inside the actual steel canister. The chemical durability of the parent glasses, as well as CCC-treated samples, has been determined using the Product Consistency Test (PCT-B) as per the standard waste disposal criteria [48]. For the better understanding of the long-term impact of CCC treatment on the dissolution rates, and to assess the possibility of a resumption of rapid dissolution in these glasses in the later stages of dissolution, the duration of PCT experiments has been extended from the normal 7-day period to 120 days in the present study. Furthermore, magic angle spinning nuclear magnetic resonance (MAS NMR) spectroscopy and fictive temperature measurements have been conducted on selected parent glasses and their respective CCC-treated analogues to investigate the correlations between the changing molecular structure of glasses as a function of thermal history and their impact on chemical durability.

2. Experimental methods

2.1. Synthesis of glasses

The compositions of the glasses investigated in this study are presented in Table 1. The baseline glass with composition (mol.%) 12.09 $\label{eq:Li2O} \text{Li}_2\text{O} - 14.57 \ \text{Na}_2\text{O} - 20.19 \ \text{Al}_2\text{O}_3 - 17.85 \ \text{B}_2\text{O}_3 - 35.29 \ \text{SiO}_2 \ \text{has been}$ labeled as BL. While BL glass is peralkaline, i.e., [(Na+Li)/Al > 1], the glasses MA-1 and Alum-1 have been designed in the metaluminous, i.e., (Na+Li)/Al = 1, and peraluminous, i.e., (Na+Li)/Al < 1, regions by changing the (Na+Li):Al ratio in the BL glass (the concentration of other constituents in the glass being constant). Further, the B2O3:SiO2 ratio has been varied in all the three abovementioned regimes by ± 5 mol.% substitution of SiO₂ with B₂O₃ in the BL, MA-1 and Alum-1 compositions to obtain peralkaline (Alk-1 and Alk-2), metaluminous (MA-x) and peraluminous (Alum-x) compositions, respectively. Additionally, the Al₂O₃:B₂O₃ ratio is varied with respect to the BL composition to create AB-1, AB-2, and AB-3 (referred as AB-x series) compositions. Lastly, the variation of the SiO₂:Al₂O₃ ratio in BL leads to the creation of SA-1, SA-2 and SA-3 (SA-x) glass compositions.

Batches (corresponding to 200 g glass as per compositions presented in Table 1) comprising Li $_2$ CO $_3$ (ACROS Organics; pure; 99%), SiO $_2$ (Alfa Aesar; >99.5%), Na $_2$ SiO $_3$ (Alfa Aesar; Anhydrous; 99%), Al $_2$ O $_3$ (ACROS Organics; extra pure; 99%), and H $_3$ BO $_3$ (ACROS Organics; extra pure; 99+%) powders were melted in 90%Pt–10%Rh crucibles in an electric furnace at temperatures varying between 1200 and 1450 °C for 1 h. The

Table 1Batched compositions of glasses (mol.%).

	${\rm Li_2O}$	Na ₂ O	Al_2O_3	B_2O_3	SiO_2
BL	12.09	14.57	20.19	17.85	35.29
Alk-1	12.09	14.57	20.19	22.85	30.29
Alk-2	12.09	14.57	20.19	12.85	40.29
MA-1	10.62	12.80	23.43	17.85	35.29
MA-2	10.62	12.80	23.43	22.85	30.29
MA-3	10.62	12.80	23.43	12.85	40.29
Alum-1	9.82	11.84	25.19	17.85	35.29
Alum-2	9.82	11.84	25.19	22.85	30.29
Alum-3	9.82	11.84	25.19	12.85	40.29
AB-1	12.09	14.57	30.19	7.85	35.29
AB-2	12.09	14.57	25.19	12.85	35.29
AB-3	12.09	14.57	15.19	22.85	35.29
SA-1	12.09	14.57	27.69	17.85	27.79
SA-2	12.09	14.57	25.19	17.85	30.29
SA-3	12.09	14.57	15.19	17.85	40.29

glass melts were air-quenched by pouring onto a stainless-steel plate. To improve the homogeneity and to eliminate undissolved solids, the glasses from the first melt were ground to powder in a tungsten carbide mill (~4 min) and then re-melted at the same temperature as the first melt. All the glasses were subsequently poured onto a stainless-steel plate. The resulting glasses were found to be visually free of undissolved solids and XRD amorphous as shown in Figure S1. The X-ray diffraction (XRD) was performed using a Bruker D8 Advance X-ray diffractometer (Bruker AXS Inc., Madison, Wisconsin; Cu K_{α}). The data was recorded over a 2θ range of 5 to 70° (step size 0.0151° and 53.1 s time per step). The glass transition temperatures of all the samples were determined using differential thermal analyzer (TA Instruments Q600 DTA/TGA, New Castle, DE), as shown in Table S1. Subsequently, all samples were annealed by holding at 50 °C below their respective glass transition temperatures for 6 h to minimize residual stress and then cooled to room temperature at 1 °C/min.

2.2. Canister centerline cooling (CCC) treatment

The parent glasses have been thermally treated following the standard canister centerline cooling (CCC) procedure for WTP HLW glasses [49]. To conduct this test, ~30 g of glass frit is loaded into boats made of 90% Pt-10% Rh sheets and covered with lids made from the same material. These boats are placed in an electric furnace pre-heated in the range of 1100 - 1300 °C, depending on melt temperature. The melt is cooled to room temperature following the CCC schedule shown in Table 2 [50]. The samples obtained from CCC heat-treatment have been divided into three portions. The first portion has been crushed to powder of particle size $< 75 \mu m$ for qualitative and quantitative phase analysis by XRD. 5 wt% ZnO is added as an internal standard for the quantitative phase analysis of the CCC samples found to be crystalline during qualitative phase analysis. The details of the XRD data collection for qualitative and quantitative phase analysis are the same as described in the previous section except that the time per step was doubled. The quantitative phase analysis has been performed using the Rietveld analysis method in TOPAS software to obtain the content of crystalline and amorphous phases in wt.%. The second portion of the powdered specimen has been sieved to obtain glass grains with particle size in the range of 75 μm to 150 μm for the glass dissolution experiments. The third portion of the sample was cut and polished (grinding on SiC paper and polishing using 1 μ m diamond suspension) to a 1 cm \times 1 cm \times 1 cm cube to be included in the glass dissolution experiments. Each sample cube was coated with silicone RTV gel on the edges of the two polished faces before placement into the dissolution vessel to obtain an observable contrast between unaltered and altered surfaces at the conclusion of the PCT experiment.

2.3. Glass dissolution experiments – product consistency test method B

The PCT, as described in detail in ASTM C1285 – 14 [48], provides a measure of the chemical durability of glass and ceramic waste forms by

 Table 2

 Canister centerline cooling (CCC) heat treatment schedule.

Segment	Start time, min	Start temperature, °C	Rate, °C/min	End time, min	End temperature, °C
				0	1150
1.	0	1150	0	30	1150
2.	30	1150	-12.5	38	1050
3.	38	1050	-1.56	83	980
4.	83	980	-0.81	145	930
5.	145	930	-0.59	238	875
6.	238	875	-0.39	367	825
7.	367	825	-0.25	565	775
8.	565	775	-0.28	745	725
9.	745	725	-0.30	1814	400

measuring the concentration of the chemical species released to a test solution under carefully controlled conditions. While Test Method A specifies that the test must be conducted for a duration of 7 days, Test Method B allows testing at various durations, temperatures, particle size and amount of glass samples, leachant volumes, and leachant compositions.

In the present study, the chemical durability of both parent and CCCtreated samples was studied using the PCT Test Method B. Accordingly, a total of 32 experiments were conducted comprising 15 parent samples, 15 CCC samples, and 2 blanks (which do not contain any glass). The PCT was performed at 90 \pm 2 $^{\circ}\text{C}$ in ASTM-Type 1 water. The static test was conducted in Polytetrafluoroethylene (PTFE) vessels that were cleaned as per the guidelines suggested in the standard ASTM C1285. For each PCT, 3.0 g glass powder (particle size: 75 μm to 150 μm ; washed and dried as per the guidelines suggested in ASTM C1285) was added to the alteration vessel along with the glass cubes, and 30 g deionized (DI) water. All the tests targeted a 2000 m^{-1} (\pm 5) surface area of sample-to-volume ratio of the solution (S/V) based on calculated surface geometry. Since a 1 cm \times 1 cm \times 1 cm cube will have a S/V of 100 m $^{-1}$, it is expected to exhibit an insignificant impact on the S/V conditions of the experiment. The density values of all the samples, as measured using the Archimedes method (in ethanol) for estimating the S/V, are reported in **Table S2.** The vessel is then sealed and kept in an oven at 90 \pm 2 $^{\circ}$ C.

All the experiments were sampled at 1, 3, 7, 28, 56, 70, 90, and 120 days. At the time of sampling, $\approx 250~\mu L$ aliquots were withdrawn, their masses were recorded, and they were immediately diluted and acidified with $\approx 0.3~\text{mol}~L^{-1}$ HNO3 (BDH Aristar® Plus trace metal grade). The pH was measured at the test temperature (hereafter denoted "pHT $^{\circ}\text{C}$ ") directly in the alteration vessel, with a glass pH meter (AccumetTM) calibrated at the same temperature with standard pH buffers. The calibration was checked with an independent set of buffers to be within 0.2 pH units of the nominal pH value. Therefore, \pm 0.2 pH unit error has been assigned to all measured values. The vessel mass was recorded before and after sampling. Ultrapure deionized water was added to the vessel to compensate for the solution lost only to evaporation and not the sampling volume.

The diluted solution aliquots were then quantitatively analyzed for the elemental concentrations of Li, Na, Al, B and Si by ICP-OES using a PerkinElmer Optima 8300 spectrometer with a Perkin Elmer SC-2 DX auto-sampler. The calibrations were performed between 1 ppm and 200 ppm depending on the element. The calibration verification was performed by running single element standards of 1000 $\mu g/mL$ concentration from Spex Certiprep (Metuchen, NJ) to verify that they were within $\pm 10\%$ of the target value. The calibration blanks were periodically used once after every 10 samples to ensure background signals and potential carryover effects were not a factor. The error on the ICP-OES measurements is \pm 10%, the maximum acceptable for calibration verification. Further dilution was necessary to match the required sample volume used by the instrument. Hence, the samples were diluted by adding ~ 7 mL DI water (> 18.0 MΩcm).

2.4. Glass dissolution parameter calculation

The mass of each element (*El*) released from the glass was calculated using a combination of recorded masses (vessel, solution, ICP-OES aliquots, and sample solids), which was then normalized to determine the glass dissolution parameters (normalized mass losses and dissolution rates). As the glass/alteration layer interface recesses when the glass dissolves, the surface area of glass exposed to the water is reduced. Similarly, the fraction of remaining unaltered glass also changes with time as the corrosion of glass particles progresses. This fraction can be calculated by designating an element that is not retained in any of the post-dissolution products as an "alteration tracer." Parruzot et al. [51] have described a set of formulae (discussed below) to account for this reduction in the surface area of the glass particles and the changing fraction of unaltered glass, which have been utilized in this present

study. ICP-OES and XRD analyses of post-dissolution products have shown that lithium is suitable for using as an "alteration tracer." For a glass dissolution experiment, the mass of each element El released from the glass throughout the experiment until sampling number n at time t_n [$m_{released}(El,t_n)$, in g] is calculated as indicated in Eq. (1), where $C_{vessel}(El,t_l)$ (in mg/L, or ppm) is the concentration of element El in the dissolution vessel at time t_i (in d); $m_{SOL,vessel}(t_i)$ (in g) is the mass of solution in the vessel at time t_i before sampling; and, $m_{SOL,sampled}(t_i)$ (in g) is the mass of solution sampled for the ICP-OES aliquot at time t_i .

$$m_{released}(El, t_n) = \frac{m_{SOL, vessel}(t_n) \times C_{vessel}(El, t_n)}{10^6} + \sum_{i=0}^{n-1} \left(\frac{m_{SOL, sampled}(t_i) \times C_{vessel}(El, t_i)}{10^6} \right)$$
(1)

To calculate the fraction of unaltered glass remaining at time t_n at sampling n [$f_{remaining}(t_n)$, unitless], Eq. (2) is used as shown below:

$$f_{remaining}(t_n) = 1 - \frac{\frac{m_{released}(Li, t_n)}{f_{element}(Li)}}{m_{glass}(t_0)}$$
(2)

where $m_{released}(\text{Li},t_n)$ (in g, from Eq. (1)) is the mass of Li released at time t_n , $f_{element}(\text{Li})$ is the mass fraction of Li in the glass (unitless); and $m_{glass}(t_0)$ is the mass of glass initially added in the experiment (in g). As mentioned above, the surface area of glass exposed to water reduces as the glass particles are altered. This is particularly significant during Stage III alteration, as the glass alteration rate increases again. Thus, the surface area of glass exposed to the fluid at sampling n at time t_n [$S_{glass}(t_n)$, in m²] is calculated for each sampling using Eq. (3) as follows:

$$S_{glass}(t_n) = \frac{6}{\rho_{glass} \times d_{glass}} \times \left[m_{glass}(t_0) \times f_{remaining}(t_n) \right]^{\frac{2}{3}} \times \left[m_{glass}(t_0) \right]^{\frac{1}{3}}$$
 (3)

where ρ_{glass} is the glass density (in $g \bullet m^{-3}$); d_{glass} (in m) is the average diameter of the glass particles (calculated from the size fraction of the glass) added to the experiment at time t_0 ; $m_{glass}(t_0)$ is the mass of glass initially added in the experiment (in g); and $f_{remaining}(t_n)$ [unitless, Eq. (2)] is the fraction of unaltered glass remaining at time t_n at sampling n. This allows the calculation of the normalized mass loss at time t_n (from experiment start through sampling n) based on the release of element El in solution $[NL(El,t_n)$, in $g \bullet m^{-2}$] using Eq. (4):

$$NL(El, t_n) = \frac{m_{released}(El, t_n)}{S_{glass}(t_n) \times f_{El}}$$
(4)

where f_{El} is the mass fraction of element El in the glass (calculated from the glass composition), while $m_{released}(El,t_n)$ and $S_{glass}(t_n)$ are calculated in Eqs. (1) and (3) respectively. From the normalized mass loss of lithium tracer, the dissolution rate is calculated based on the release of an element El [r(i), in $g \cdot m^{-2} \cdot d^{-1}$] over any duration throughout the experiment using Eq. (5). Accordingly, two dissolution rates – (i) "28-d rate" which uses normalized loss values from 1 to 28 days, and (ii) "longer-term rate," which uses normalized loss values from 28 to 90 days, have been calculated in this study.

$$r(El) = \frac{\Delta[NL(El,t)]}{\Delta t} \tag{5}$$

2.5. Electron microscopy

To perform microstructural observations on the CCC samples, a part of the glass/glass-ceramic was chemically etched using 2 vol.% HF (aq.) for 1 min, followed by cleaning using DI water and ethanol. The sample was then dried for at least 24 h before mounting on metallic stubs and sputter-coated with a 10-nm thick gold coating.

In the case of post-dissolution samples, since the cubes included in the PCT vessel had been coated with silicone RTV adhesive on two of the edges on one face, the adhesive was removed after completion of the PCT experiments. The cubes were then cut to obtain a cross-section for observation under scanning electron microscope (SEM). The cubes obtained at the end of PCT were analyzed in two ways-(1) the cross-section was polished and mounted into a resin mold to locate the characteristic alteration layer and (2) the face that had been partially coated with silicone RTV adhesive was studied to observe differences in the altered and unaltered surface of the cube. The samples were mounted on metallic stubs followed by sputter-coating with a 10 nm thick gold coating.

The microstructure of the glass/glass-ceramic samples (pre- and post-corrosion) was investigated using a field emission – scanning electron microscopy (SEM; ZEISS Sigma FE-SEM; acceleration voltage 10 kV) operated in secondary electron imaging mode. The elemental distribution mapping was performed by energy dispersive spectroscopy (EDS; X-Max Oxford Instruments; Aztec software).

2.6. Magic angle spinning – nuclear magnetic resonance spectroscopy

The structure of selected glasses and glass-ceramics has been studied using multi-nuclear magic angle spinning - nuclear magnetic resonance (MAS NMR) spectroscopy. The MAS NMR spectra of ¹¹B and ²⁷Al have been acquired using a commercial spectrometer (DD2, Agilent) and 3.2 mm MAS NMR probe (Agilent). The unaltered glasses were powdered in an agate mortar, packed into 3.2 mm zirconia rotors, and spun at 20 kHz for ¹¹B MAS NMR and 22 kHz for ²⁷Al MAS NMR. ²⁷Al MAS NMR data have been acquired at 16.4 T (182.34 MHz resonance frequency) using RF pulses of 0.6 μ s (equivalent to a $\pi/12$ tip angle), recycle delays of 2 s, and signal averaging of 1000 acquisitions. The acquired data has been processed without additional apodization and referenced to aqueous aluminum nitrate at 0.0 ppm. ¹¹B MAS NMR experiments were conducted at 16.4 T (224.52 MHz resonance frequency), incorporating a 4 s recycle delay, short rf pulses (0.6 μ s) corresponding to a $\pi/12$ tip angle, and signal averaging of 400 to 1000 scans. The acquired spectra have been processed with minimal apodization and referenced to aqueous boric acid (19.6 ppm). Fitting of the MAS NMR spectra was performed using DMFit [52] and, accounting for distributions in the quadrupolar coupling constant, the CzSimple model has been utilized for ²⁷Al MAS NMR spectra. The "Q MAS 1/2" and Gaus/Lor functions are used to fit 3and 4-fold coordinated boron resonances in the 11B MAS NMR data, respectively, and N₄ (BO₄/(BO₃ + BO₄)) is calculated from the relative areas of these peaks, with a small correction due to the overlapping satellite transition of the 4-fold coordinated boron peak [53].

2.7. Fictive temperature measurements

The specific heat capacity (Cp) of the glasses (before and after CCC treatment) was measured utilizing a differential scanning calorimeter (DSC; NETZSCH Pegasus 404 C). The absolute value of $C_{\rm p}$ was determined by subtraction of the empty Pt crucible baseline and adjustment of the heat flow values based on sapphire standard runs and corresponding literature values. The enthalpic fictive temperature (T_f) of the samples was calculated by analysis of the temperature dependent specific heat capacity using the unified enthalpy matching method [54, 55]. First, glasses were heated from room temperature to the supercooled liquid region above the glass transition temperature, with a heating rate of 20 °C/min, to obtain the original thermal-history-dependent C_p curve. Then, glasses were held isothermally at the equilibrium supercooled liquid region for 2 min to erase their thermal history. After that, the glasses were cooled from the supercooled liquid to room temperature at a cooling rate of 20 °C/min. Finally, glasses were reheated from room temperature to the supercooled liquid region above the glass transition temperature at the heating rate of 20 $^{\circ}\text{C/min}$ to obtain the C_p curve dependent on the thermal history defined by the 20 $^{\circ}\text{C/min}$ cooling rate. The second C_p curve can be used to estimate the fictive temperature of the defined thermal history, applying Moynihan's fictive temperature calculation method [56]. The area between the two Cp curves

corresponds to the enthalpy difference between the two non-equilibrium states, which is proportional to the fictive temperature difference. The fictive temperature of the original thermal history was estimated by shifting the fictive temperature, as described by Guo et al. [54]. The standard deviation associated with the measurement and calculation of fictive temperature in this study is $\pm 2.5~^{\circ}\text{C}.$

3. Results and discussion

3.1. Compositional analysis of glasses

The compositional analysis has been performed on selected glasses to account for any loss of B_2O_3 , Li_2O and Na_2O due to volatilization from the melt. Accordingly, Table 3 presents the as measured concentrations of B_2O_3 , Li_2O and Na_2O in five glass samples, namely BL, Alk-1, AB-1, MA-1 and Alum-3. As evident, the analyzed compositions are in good agreement (within $\pm 10\%$) with the batched compositions thus indicating minimal losses due to volatilization. The small losses of Li_2O and Na_2O , as observed in the analyzed compositions, can be attributed to the relatively high temperatures required to melt the respective batches. Nevertheless, these deviations are insignificant and unlikely to impact the trends in the compositional dependence of the properties presented in this study.

3.2. Compositional dependence of crystallization in glasses

3.2.1. Effect of varying (Li+Na):Al ratio

Fig. 1 presents the X-ray diffractograms of the CCC-treated samples, while Table 4 presents the results of the quantitative phase analysis. All three baseline glasses with varying alkali–to–alumina ratios, i.e., BL (Fig. 1a), MA-1 (Fig. 1b) and Alum-1 (Fig. 1c) demonstrate high resistance towards devitrification. The peralkaline baseline glass, BL, is slightly crystalline, with 3 wt.% nepheline (Na_{7.15}Al_{7.2}Si_{8.8}O₃₂; PDF #97–006–5960; hexagonal) formation from the CCC test. The metaluminous baseline glass, MA-1, is completely amorphous, while the peraluminous baseline glass, Alum-1, forms 5.4 wt.% corundum (Al₂O₃; PDF #97–006–3647; hexagonal) during the CCC test. In simplistic terms, the suppression of crystallization in these glasses is not surprising owing to their high B₂O₃ content [16, 27]. However, to ascertain the exact reason for this effect is highly complex, as has been discussed in Deshkar et al. [15], and requires detailed structural and thermodynamic investigations that are beyond the scope of the present study.

In brief, the composition of glass MA-1 (mol.%, $10.62 \text{ Li}_2\text{O} - 12.80 \text{ Na}_2\text{O} - 23.43 \text{ Al}_2\text{O}_3 - 17.85 \text{ B}_2\text{O}_3 - 35.29 \text{ SiO}_2)$ is very similar to the glass SB-15 (mol.%, $25 \text{ Na}_2\text{O} - 25 \text{ Al}_2\text{O}_3 - 15 \text{ B}_2\text{O}_3 - 35 \text{ SiO}_2)$ investigated by Deshkar et al. [15], the major difference being that the 23.24 mol.% alkali oxide in the glass MA-1 has been divided among Li₂O and Na₂O. Assuming that the alkali oxides in both studies exhibit a similar structural role, i.e., charge compensating AlO₄ units [(Na+Li)/Al \approx 1], based on the results from Deshkar et al. [15], at first glance, we expect the glass MA-1 to devitrify. However, the results in the present study seem counterintuitive. When investigating the chemical make-up and thermal treatment (isothermal heat-treatment of glass SB-15 at 850 °C vs. slow cooling of melt–to–glass in CCC treatment) of the two glasses, the following structural differences can be anticipated (based on the

Table 3Composition of selected glasses as analyzed using ICP-OES.

		Composi BL	itions Alk-1	AB-1	MA-1	Alum-3
Li ₂ O	wt.% (batched)	5.40	5.36	5.15	4.63	4.25
	wt.% (analyzed)	5.12	5.32	5.65	3.50	4.07
Na ₂ O	wt.% (batched)	13.51	13.41	12.88	11.56	10.62
	wt.% (analyzed)	11.31	13.49	14.22	8.71	10.34
B_2O_3	wt.% (batched)	18.58	23.62	7.80	18.11	12.94
	wt.% (analyzed)	16.93	22.85	7.79	16.94	11.88

literature).

- (1) The assumption that both Li₂O and Na₂O exhibit the same role in the glass structure is likely to be incorrect. The glass MA-1 is expected to be more heterogeneous when compared to the glass SB-15 (from Deshkar et al. [15]), as Li₂O comprises ~45% of the total alkali content in the former. The presence of Li₂O (Li⁺ being a higher field strength cation compared to Na⁺) is known to reduce the Si/B mixing in the glass network, increase the coordination of Na⁺, impact the ratio of ring-to-non-ring BO₃ units, and induce the formation of five-coordinated aluminum in the glass structure [57-59]. The results in the present investigation are in good agreement with the literature [13, 45, 58, 60], as ¹¹B and ²⁷Al MAS NMR spectroscopy results (presented in Figs. 2a and 2b and Table 5) confirm the presence of small fractions of BO₄ and AlO₅ units in the structure of metaluminous glasses. The above discussed structural variations due to the substitution of Na⁺ by Li⁺ in the glasses are expected to have a significant impact on their transport properties (viscosity, diffusivity and conductivity), as has been shown by Mysen [61] in the case of aluminosilicate glasses and melts, thus impacting their crystallization behavior.
- (2) When comparing the process of heat-treatment in the two investigations (present vs. Deshkar et al. [15]), the structure of the MA-1 glass melt (during the CCC treatment) is expected to have a higher concentration of Al-O-Al, B-O-B, Si-O-B^[3] and Si-O-Si bonds when compared to Si-O-Al linkages. According to Dubinsky and Stebbins [62], the reaction 2 Al–O–Si \leftrightarrow Al–O–Al +Si-O-Si shifts to the right with increasing temperature in the aluminosilicate melt, while according to Moncke et al. [35, 63], the structure of slow cooled, well-annealed (as in the case of CCC treatment) alkali-poor [$R = (Na_2O + Li_2O)/B_2O_3 < 0.5$] borosilicate glasses is dominated by homopolar B-O-B and Si-O-Si linkages along with Si-O-B^[3] bonds. As has been discussed in our previous article [15], the presence of Si-O-Al linkages in the glass structure is crucial for the crystallization of nepheline. Therefore, their reduced concentration in the MA-1 glass melt may be one of the reasons for the suppression of nepheline crystallization.

The above discussed differences in the structure of MA-1 and SB-15 glasses and melts highlight a complex picture that warrants a comprehensive structural study elucidating the impact of composition and thermal treatment on the short–to–medium range ordering in the structure of these glasses and melts.

In the case of the peralkaline glass, BL, the crystallization of a minor amount of nepheline may be attributed to the higher concentration of Si-O-Al linkages (compared to glass melt MA-1) as most of the aluminum in the glass is expected to be tetrahedrally coordinated. It has been reported in the case of Na₂O-Li₂O-B₂O₃-SiO₂ glass system that BO₄ units are preferentially charge compensated by Na⁺, while Li⁺ tends to associate with non-bridging oxygens (NBOs) in the borosilicate network [64]. Similar results have been reported in the case of Na₂O-CaO-Al₂O₃-B₂O₃-SiO₂ glasses, where the high field strength cation, i.e., Ca²⁺, shows a strong preference to associate with non-bridging oxygens (NBOs), while more of the oxygens around Na⁺ are bridging oxygens (BOs) [45]. Assuming the same result to be valid in the glasses investigated in the present study, the AlO₄ units in the glass BL are expected to be preferentially charge compensated by Na⁺ (owing to higher Na/Al ratio when compared to glass MA-1), thus, providing a pathway towards nepheline crystallization.

 $^{^1}$ The glass MA-1 can be considered as alkali-poor borosilicate glass as, ideally, all the alkali cations should be charge compensating AlO₄ units. Therefore, it should not have any Na $^+$ or Li $^+$ to convert BO₃ \rightarrow BO₄.

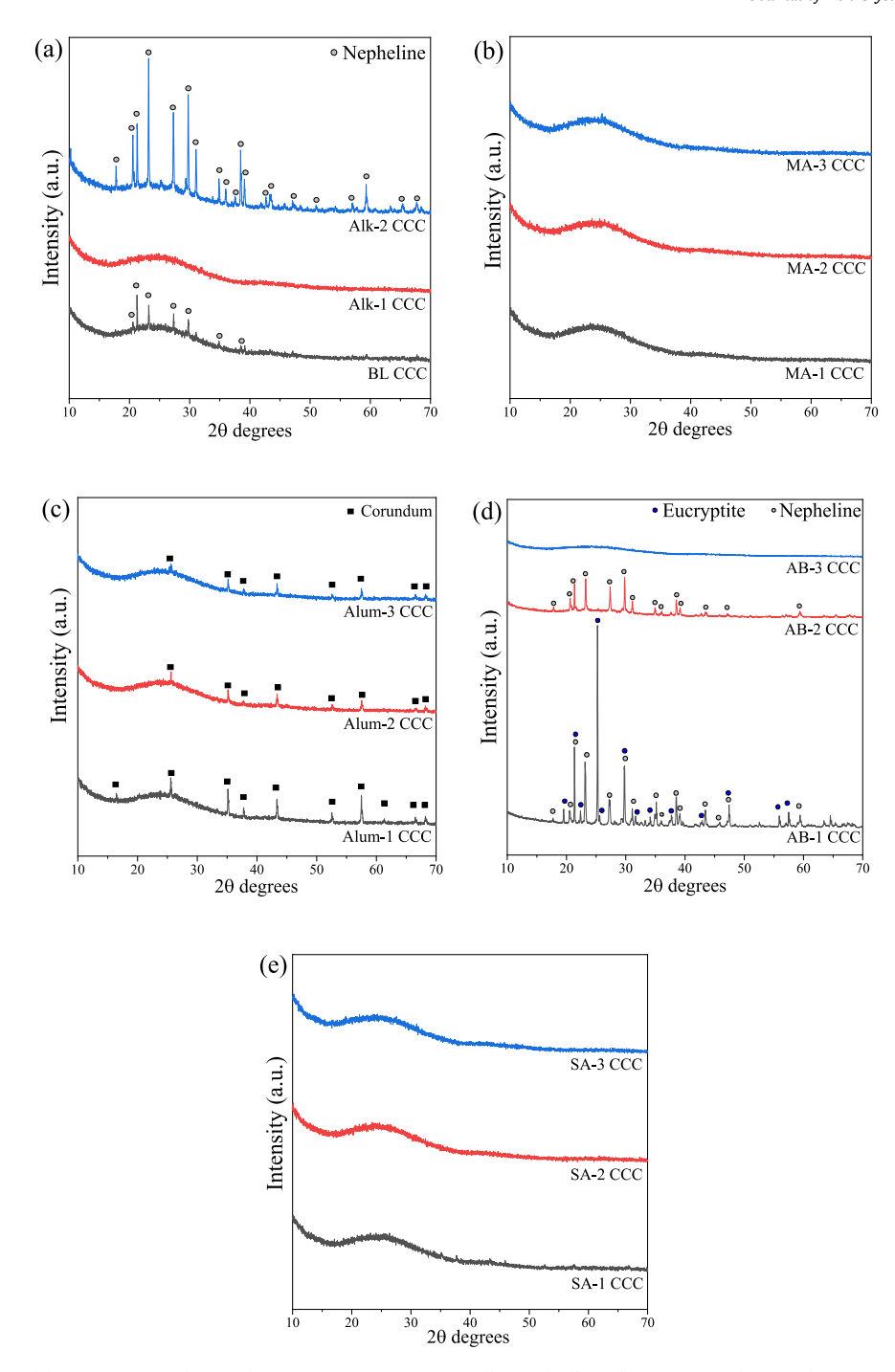


Fig. 1. X-ray diffractograms of glasses after CCC treatment: (a) BL, Alk-1 and Alk-2; (b) MA-x; (c) Alum-x; (d) AB-x; (e) SA-x series.

	wt.%*					vol.% crystal in CCC
	Nepheline ($Na_{7.15}Al_{7.2}Si_{8.8}O_{32}$)	Eucryptite (LiAlSiO ₄)	Corundum (Al ₂ O ₃)	others	Amorphous	•
BL CCC	3.0	_	_	-	97.0	2.80
Alk-2 CCC	26.3	0.6	_	_	73.1	26.5
AB-1 CCC	54.8	17.7	7.5	4.5 (sodium silicate)	15.5	84.4
AB-2 CCC	28.6	_	_	0.6 (tridymite)	70.8	28.2
Alum-1 CCC	_	_	5.4	0.9 (Aluminum borate)	93.7	6.97
Alum-2 CCC	_	_	2.6	_	97.4	1.98
Alum-3 CCC	_	-	3.2	-	96.8	2.74

 $^{^{\}ast}$ All other samples were XRD amorphous after CCC, as shown in Fig. 1.

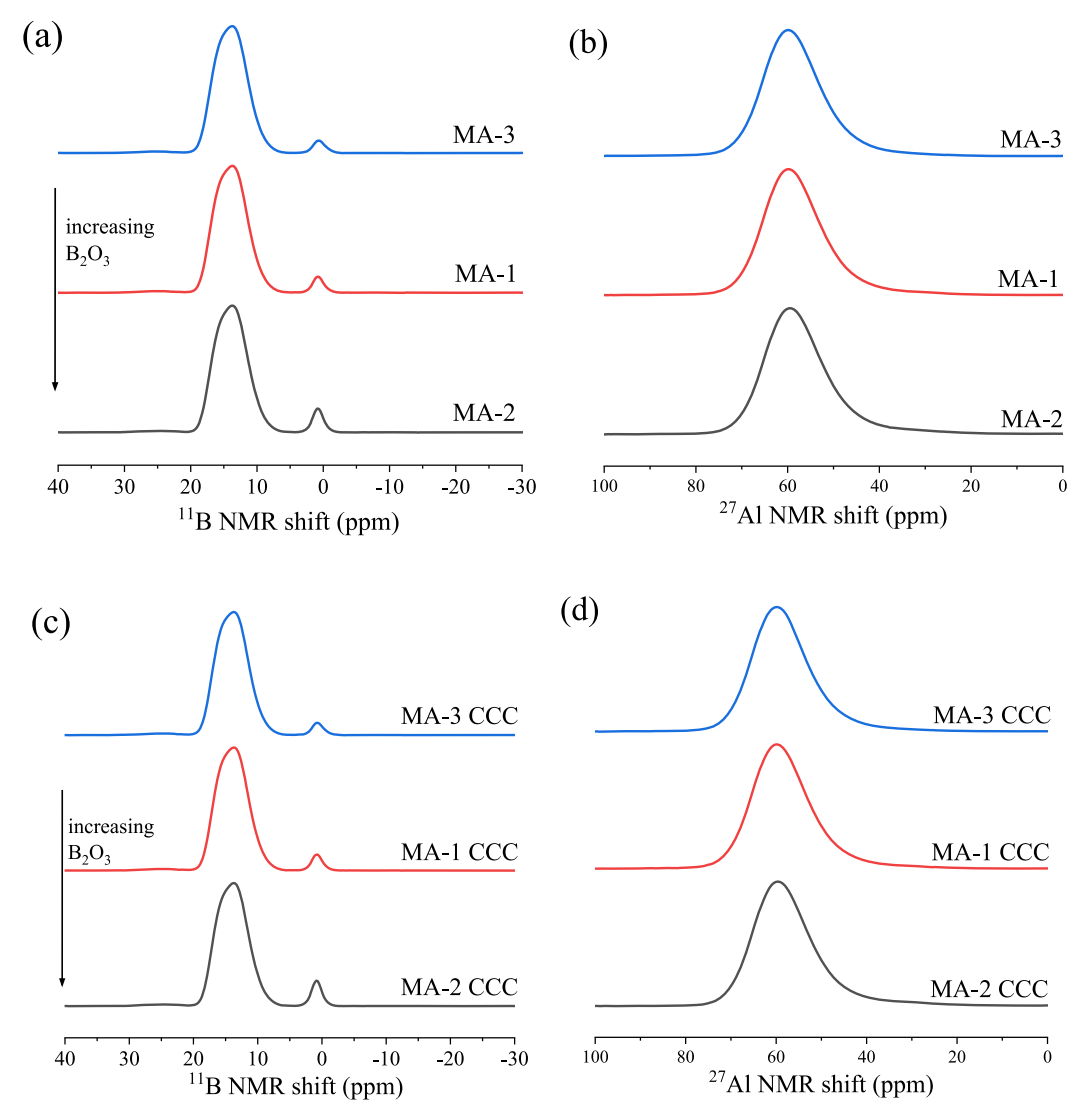


Fig. 2. (a) ¹¹B and (b) ²⁷Al MAS NMR spectra of parent MA-x glasses; (c) ¹¹B and (d) ²⁷Al MAS NMR spectra of CCC-treated MA-x glasses.

Table 5 Boron speciation as denoted by N_4 (=[BO₄]/([BO₃]+[BO₄])) obtained from ^{11}B MAS NMR and % content of five-coordinated aluminum as obtained from ^{27}Al MAS NMR (Standard deviation: $\pm 1\%$).

	N ₄	⁵ [A <i>l</i>]%
MA-1 glass	0.043	2.6
MA-1 CCC	0.044	2.5
MA-2 glass	0.062	3.7
MA-2 CCC	0.065	3.3
MA-3 glass	0.036	2.4
MA-3 CCC	0.035	1.6
Alum-1 glass	0.016	6.7
Alum-2 glass	0.030	6.5
Alum-3 glass	0.013	3.6

For the peraluminous glass Alum-1, while the majority of Al^{3+} will be four-fold coordinated, a significant fraction of aluminum is expected to exist in five-fold coordination due to (1) the deficit of alkali cations required to charge compensate four-fold aluminate units [65], and (2) high ionic field strength of Li^+ (as has been observed in the case of metaluminous glasses). Therefore, the crystallization of \sim 5 wt.% corundum in glass Alum-1 may be attributed to the higher fraction of five-coordinated aluminum in the glass structure, and the higher fraction of Al–O–Al linkages in the melt (compared to Si–O–Al linkages)

during the CCC treatment [62]. The ²⁷Al and ¹¹B MAS NMR results on the glass Alum-1, as presented in **Fig. 3** and **Table 5**, support our hypothesis as 6.7% of aluminum in this glass is five-coordinated, while the majority of boron is three-coordinated.

3.2.2. Effect of varying B₂O₃:SiO₂ ratio

In peralkaline glasses, BL, Alk-1, and Alk-2, the effect of CCC treatment clearly shows that a lower B2O3 content (Alk-2) promotes crystallization of nepheline and eucryptite phases, while a high B2O3 content (Alk-1) suppresses crystallization, as shown in Fig. 1a. Table 4 shows the quantitative crystalline phase assemblage of these samples as determined using Rietveld analysis. Nepheline (Na_{7,15}Al_{7,2}Si_{8,8}O₃₂; PDF #97-006-5960; hexagonal) is detected as the preferred crystal phase, while eucryptite (LiAlSiO₄; PDF #97-003-2595; hexagonal) is present in minor quantities, even though Li_2O and Na_2O are both present almost in equimolar concentrations (Na₂O/Li₂O \approx 1.20) in the glass composition. The preference of crystallization of nepheline over eucryptite may be attributed to the formation of Al-O-Si linkages in the glass structure where AlO₄ tends to be preferentially charge compensated by Na⁺, while Li⁺, being a higher ionic field strength cation, tends to associate with NBOs concentrated primarily in the silica rich phase, as discussed above. Here it should be mentioned that borosilicate glasses containing both Li₂O and Na₂O have been shown to be chemically heterogeneous (nano-scale phase separation) at the intermediate-range structural level

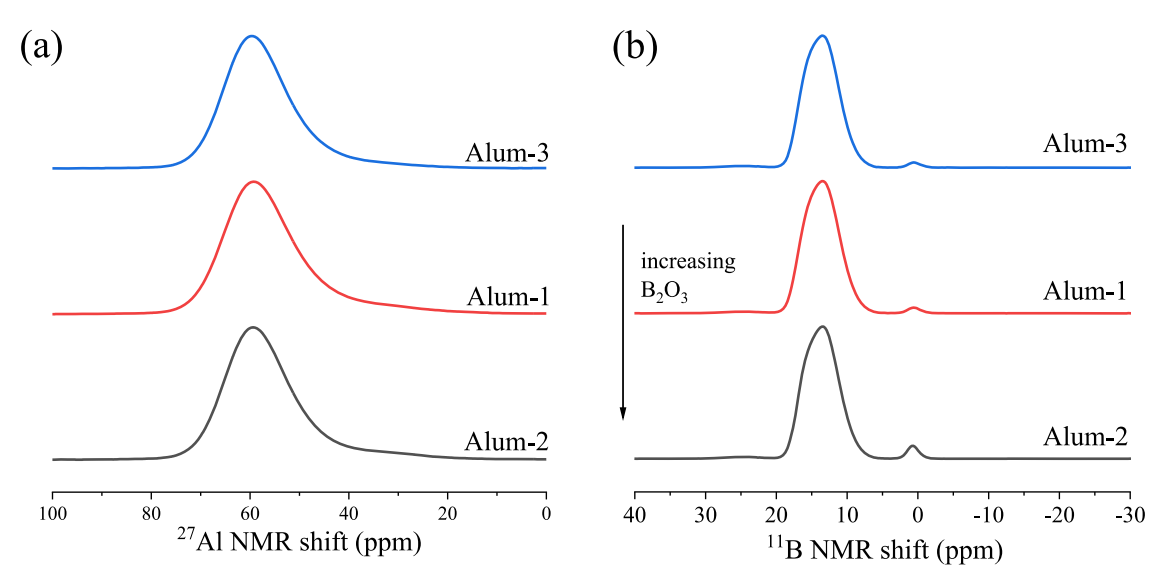


Fig. 3. (a) 27 Al and (b) 11 B MAS NMR spectra of Alum-x parent glasses.

wherein domains close to a binary (lithium-rich) alkali silicate in composition are embedded in the sodium borosilicate hosts [57]. Nevertheless, considering that ${\rm Li}^+$ is known to substitute (for Na⁺) in the oval channels of the nepheline crystal structure [18], the observed nepheline phase is possibly a solid solution of the type ${\rm Na}_{(1:x)}{\rm Li}_x{\rm AlSiO}_4$.

In metaluminous series, i.e., MA-1, MA-2, and MA-3, all the glasses remained amorphous upon CCC treatment (Fig. 1b). The results are intriguing, especially for glass MA-3, which has B₂O₃ (12.85 mol.%) content equal to that in the glass Alk-2. Further, in peraluminous glasses, i.e., Alum-1, Alum-2, and Alum-3, the impact of varying B:Si ratio seems inconsequential (from the viewpoint of their crystallization behavior) as all the samples crystallize corundum (Al₂O₃) phase with its content varying between 2 and 6 wt.% (Fig. 1c; Table 4) upon CCC treatment.

If we compare the crystalline phase evolution in the three series of glasses investigated in the present study, the following three glasses-Alk-2, MA-3 and Alum-3-exhibit an intriguing crystallization behavior (see Fig. 1; Table 4). At their structural level, these three glasses have nearly identical B_2O_3/SiO_2 (≈ 3.13) and Na_2O/Li_2O (≈ 1.20) ratios, while their (Li₂O+Na₂O)/Al₂O₃ ratio traverses through peralkaline-to-metaluminous-to-peraluminous regions. Therefore, per literature [45, 57, 58, 66], the glass MA-3 is expected to be more homogeneous (higher mixing of silicate and borate units, i.e., higher fraction of Si-O-B^[3] linkages [35]) than Alk-2 because in the metaluminous glass (MA-3), all the alkali cations are expected to charge compensate AlO₄ units. Thus, ideally, there should not be any Li₂O available to create chemical heterogeneity in the glass structure. [N.B. For simplicity, we are negating the possibility of any deviation from aluminum avoidance rule in MA-x glasses, though it has been shown that they contain small fraction of AlO₅ units (Fig. 2b; Table 5) owing to the presence of high field strength cation, i.e., Li⁺ [18, 59]]. On the other hand, assuming that all Na₂O (14.57 mol.%) and a fraction of Li₂O (5.62 mol.%) will charge compensate AlO₄ units in the Alk-2 glass, 6.47 mol. % Li₂O remains to create de-mixing of silicate and borate units in the glass network, thus, leading to a lower fraction of Si-O-B linkages [57]. Since the conversion of Si-O-Al linkages to Si-O-B linkages in the glass structure is known to suppress nepheline crystallization, this explains the suppression of crystallization in the glass MA-3. Further, when comparing the structure of glass Alum-3 with MA-3, while the fraction of Si-O-Al and Si-O-B linkages in the structure of both the glasses are expected to be (almost) the same, the glass Alum-3 exhibits a higher fraction of five- and six-coordinated aluminum in its structure (Table 5), leading to the crystallization of the corundum phase.

3.2.3. Effect of varying B₂O₃:Al₂O₃ ratio

The crystalline phase evolution in glasses (because of CCC treatment) AB-1, AB-2, and AB-3, along with the baseline glass BL, is presented in Fig. 1d, while the quantitative phase analysis is presented in Table 4. In general (and as expected), increasing B2O3:Al2O3 ratios result in the suppression of the crystallization tendency in the investigated glasses. The phase assemblage of the CCC-treated glass AB-1 comprises nepheline (\sim 55 wt.%), eucryptite (\sim 18 wt.%), and corundum (\sim 7.5 wt.%). These results are intriguing when compared to the phase assemblage of the CCC-treated glass Alum-3, as both glasses are peraluminous in nature. Nevertheless, significantly higher tendency towards devitrification of glass AB-1 compared to Alum-3 can be attributed to its lower concentration of B₂O₃ and higher (Li₂O+Na₂O)/Al₂O₃ than for the latter, thus resulting in higher fractions of Si-O-Al and Al-O-Al linkages combined with lower concentration of Si-O-B linkages in the glass structure. Overall, the crystalline phase evolution in these glasses is in good agreement with the literature [19] and can be explained based on the results presented (and discussed) in our previous studies [15, 42, 43].

3.2.4. Effect of varying Al₂O₃:SiO₂ ratio

The glasses SA-1, SA-2, and SA-3 (where Al_2O_3 :SiO₂ ratio was varied with respect to the glass BL) remained amorphous after CCC treatment (Fig. 1e), owing to their high B_2O_3 content (17.85 mol.%). These results demonstrate the effective role played by B_2O_3 in suppressing crystallization, in agreement with the literature [3, 5, 6, 16, 24, 67].

3.2.5. Implications of the results on the predicting ability of the submixture model

Among the various constraint models for predicting nepheline formation in HLW glasses, the first one was proposed by Li et al. [10] known as nepheline discriminator (ND), which is based on limiting the normalized SiO_2 concentration given by Eq. (6):

$$N_{Si} = \frac{W_{Si}}{(W_{Si} + W_{Al} + W_{Na})} \ge 0.62$$
 (6)

Here, N_{Si} is the normalized silica concentration and W_i represents weight fraction of i th species. As this model was later found to be overly conservative and did not consider the impact of other oxides present in the HLW glasses, the optical basicity (Λ_{glass}) model was later proposed by McCloy et al. [24, 68] as a supplementary constraint to include the glasses with $N_{Si} < 0.62$ that do not precipitate nepheline (Eq. (7)).

$$\Lambda_{glass} = \frac{\sum_{i} x_{i} q_{i} \Lambda_{i}}{\sum_{i} x_{i} q_{i}} < 0.55$$
 (7)

Here, q_i is the number of oxygen atoms present in the i_{th} component oxide, x_i is its mole fraction, and Λ_i is its molar basicity.

Table 6 presents the nepheline discriminator (ND) and optical basicity (OB) values of the investigated glasses, as calculated from their batched compositions using Eqs. (6) and (7), respectively. According to the ND model, nepheline is unlikely to form (upon CCC treatment) when the normalized silica content in the Na₂O–Al₂O₃–SiO₂ glass is \geq 62 wt. %. On the other hand, according to the OB model, nepheline precipitation in a glass (upon CCC treatment) is unlikely to occur if the OB value is < 0.55 [31]. Based on the criteria laid down by the ND and OB models, all the glasses in the present study should precipitate nepheline or similar phases upon CCC-treatment. However, the XRD results reveal that only four compositions, i.e., BL, Alk-1, AB-1 and AB-2, crystallize nepheline. Thus, the conservative nature and incorrect predictions of the ND and OB models are evident from the results presented in this study.

When comparing the crystallization behavior of the investigated glasses with the predictive ability of the SM model [3], even the SM model shows poor performance. Fig. 4 presents the glass compositions investigated in the present study plotted on the SM ternary diagram. The calculations for obtaining end-member compositions of the pseudo-ternary have been shown in Table S3. It should be noted here that the SM model does not only predict the probability of nepheline formation in a glass but also predicts the expected vol.% of nepheline formation upon the CCC treatment. While the model accurately predicts the propensity of nepheline crystallization in glasses BL, Alk-2 and AB-2, it failed to make similar predictions for almost all the other glasses investigated in the present study. For example, according to the model, none of the glasses investigated in the present study should turn out to be amorphous upon CCC treatment. However, there are at least 7 out of 15 investigated glasses which remained amorphous after CCC tests. Further, some of the glasses that remain amorphous (for example, SA-1) or slightly crystalline (for example, BL) upon CCC treatment should crystallize >20 vol.% nepheline as per the predictions of the SM model. Finally, the peraluminous glasses (Alum-1, Alum-2 and Alum-3) are predicted to crystallize 10 - 20 vol.% nepheline. However, they remain highly amorphous (93 vol.%) with corundum as the only crystalline phase. These results highlight that the SM model requires some refinement, specifically in the metaluminous and peraluminous compositional space.

Table 6Nepheline Discriminator (ND) and Optical Basicity (OB) values of glasses calculated based on batched compositions.

	ND	OB	Nepheline formation upon CCC?
BL	0.417	0.561	Yes
Alk-1	0.381	0.554	Yes
Alk-2	0.450	0.569	No
AB-1	0.347	0.591	Yes
AB-2	0.379	0.576	Yes
AB-3	0.464	0.546	No
SA-1	0.309	0.572	No
SA-2	0.344	0.568	No
SA-3	0.497	0.554	No
MA-1	0.400	0.557	No
MA-2	0.364	0.550	No
MA-3	0.432	0.564	No
Alum-1	0.391	0.555	No
Alum-2	0.355	0.548	No
Alum-3	0.423	0.562	No

3.3. Impact of thermal history (CCC treatment) on the structure of glasses

While the XRD allows us to follow the crystalline phase evolution in the glass-ceramics as a function of composition, it does not provide any information pertaining to the changes in the structure of samples that remain amorphous after the CCC treatment. Nevertheless, as has been shown in the literature and discussed in the introduction, the thermal history (measured in terms of fictive temperature) of a glass has a considerable impact on its dissolution kinetics [37, 38, 69]. Therefore, before we discuss the dissolution kinetics and behavior of the investigated glasses (before and after CCC), it becomes imperative to understand the impact of thermal history on the structure of glasses that did not crystallize in the CCC treatment. Accordingly, three glass compositions, MA-1, MA-2 and MA-3, were selected, as representative of all the glasses that stayed amorphous after CCC treatments, for further structural investigations.

As shown in Fig. 5, the parent glasses have a higher fictive temperature than their CCC counterparts. Since the sample undergoing the CCC treatment starts from the molten state and slowly cools to room temperature over a period of $\sim\!30$ h, this leads to a lower fictive temperature in the case of CCC-treated samples. The difference between the fictive temperatures of parent glass and its CCC-treated counterpart is the highest in the case of MA-2 sample ($\Delta T_f = \sim\!53~^{\circ}\text{C}$), which has the highest boron content. Considering that both boron and aluminum coordination in the glasses has been shown to be sensitive to their thermal history [37, 70], it is worth investigating the impact of thermal history on the structure of these glasses. Further, the differences in the T_f of parent and CCC-treated glasses are expected to manifest changes in their dissolution rates, as will be discussed in the next section.

When discussing the impact of composition, the T_f values tend to decrease with increasing B_2O_3 content in glasses. Considering that the fictive temperature of a glass is directly proportional to its glass transition temperature [71], the observed trend is expected and well explained.

Figs. 2a and 2c present the ¹¹B MAS NMR spectra of the parent and CCC-treated glasses from MA-x series, respectively. The broad asymmetric peaks between 10 ppm and 20 ppm correspond to trigonal boron (BO₃), while the ones near 0 ppm correspond to tetrahedral boron (BO₄) [44, 64]. Owing to the good resolution of the NMR spectra (due to the use of high magnetic fields), we have been able to determine the relative intensities of each species, which have been presented in Table 5. Considering the metaluminous nature of glasses in MA-x series, ideally, the presence of BO₄ units in these glasses is not expected. Therefore, the appearance of a minor fraction of BO₄ units, which increases with increasing B₂O₃ content, in the MA-x series of glasses may be attributed to the formation of small but noticeable fraction of AlO₅ units (²⁷Al MAS NMR spectra; peak assignment: 30 – 40 ppm [60, 72]; Fig. 2b; Table 5) due to the presence of Li⁺ (a high ionic field strength cation) [45, 58, 59], thus, making some alkali cations available for the charge compensation of BO₄ units instead of AlO₄ (²⁷Al MAS NMR spectra; peak assignment: \sim 60 ppm [15, 60]; Fig. 2b; Table 5).

When comparing the structure of the parent glasses in MA-x series with those passed through CCC treatment, no significant changes could be observed in the boron speciation in the glasses, as evident from Table 5. This is intriguing as boron speciation in the borosilicate glasses has been shown to be sensitive to its thermal history. Nevertheless, minimal changes in the boron speciation does not imply that no structural changes have occurred in the short – to – intermediate range ordering in the borate network of the investigated glasses. As has been reported by Moncke et al. [73] in alkali-poor borosilicate glasses (Na₂O/B₂O₃ < 0.5), although the N₄ fraction may not change as a function of thermal history (quenching of melt between two brass plates

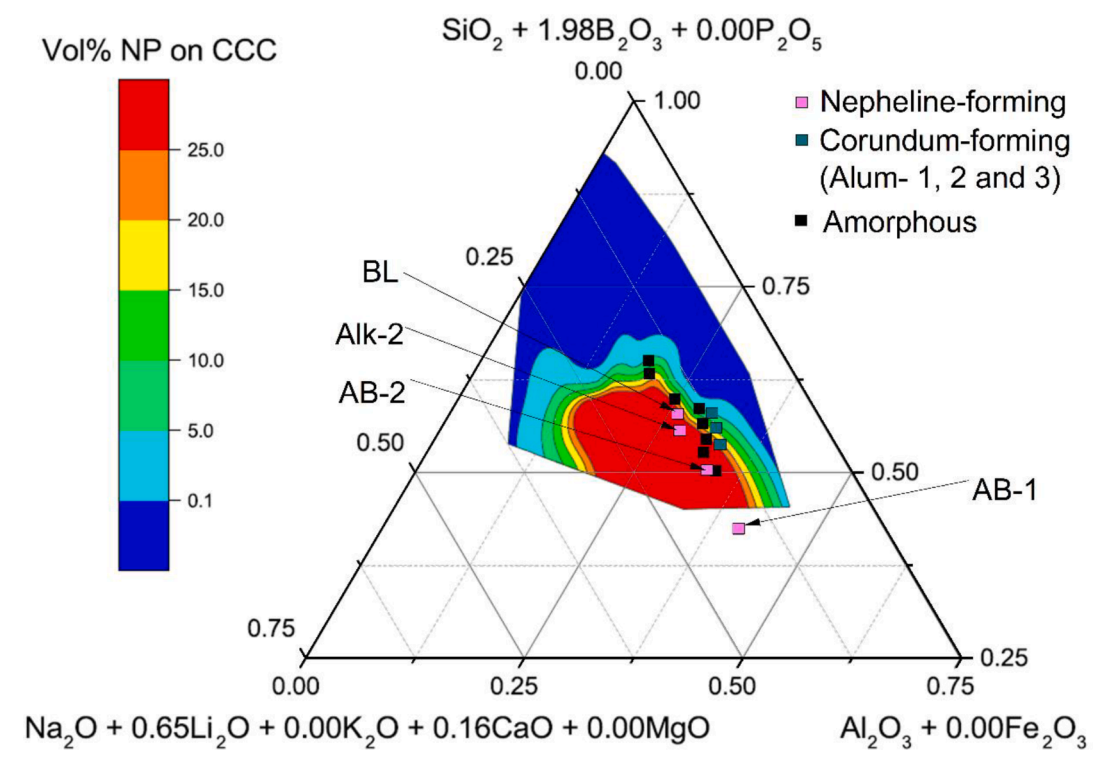


Fig. 4. Glass compositions from Table 1 plotted on a pseudo-ternary phase diagram with regions denoting different volume percent of nepheline expected to crystallize during CCC (using conservative fit). Reprinted with permission from Vienna et al. [3] Copyright (2016) The American Ceramic Society and Wiley Periodicals, Inc.

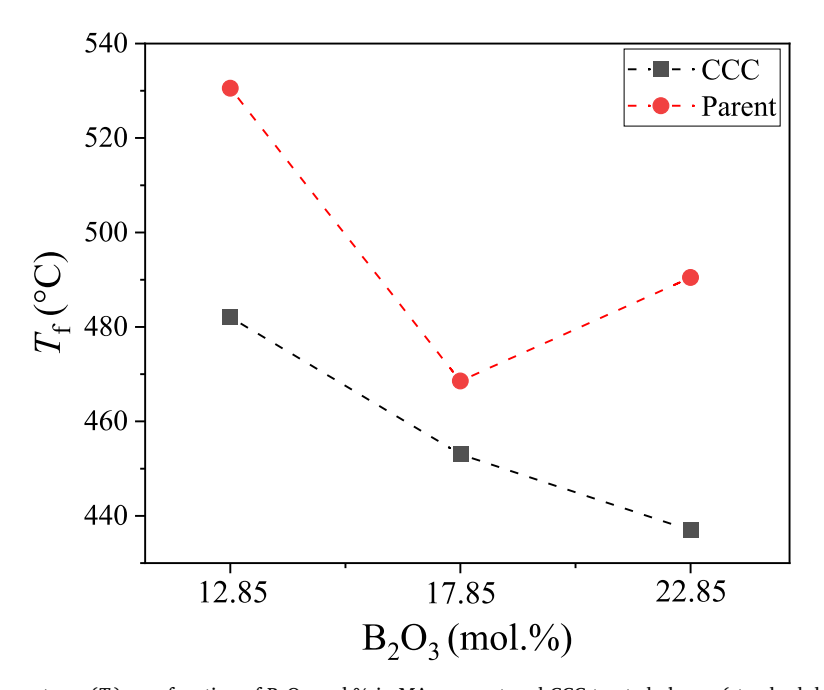


Fig. 5. Fictive temperatures (T_f) as a function of B_2O_3 mol.% in MA-x parent and CCC-treated glasses (standard deviation: ± 2.5 °C).

vs. annealing at $T_g\pm50~^{\circ}C$ for several hours), it brings a considerable change in the medium range ordering in their structure. It has been shown using 1D and 2D NMR spectroscopy that the medium-range structure of a melt-quenched alkali-poor borosilicate glass is represented by a more mixed silicate – borate network, reflected by B–O–Si bonds, while more homopolar B–O–B and Si–O–Si bonds are found in the slow-cooled/well-annealed sample [74]. As discussed earlier, the MA-x and Alum-x series of glasses can be considered as alkali-poor

borosilicates, as most alkali cations are acting as charge compensators for AlO_4^- . Therefore, one can expect the formation of more homopolar B–O–B and Si–O–Si bonds linkages in the CCC-treated samples compared to the parent glasses.

Further, the aluminum speciation in the CCC-treated glasses exhibits a slight decrease in the fraction of AlO_5 content (compared to their parent analogues), as shown in Table 5. However, the magnitude of this change in the fraction of five-coordinated aluminum in the CCC-treated

glasses decreases with increase in their B_2O_3 content (Table 5; Fig. 3). The fraction of AlO_5 units in the glass structure are known to be sensitive to the thermal history of the glass, along with the ionic field strength of non-framework cations, wherein higher fictive temperature results in higher fraction of five-coordinated aluminum [75].

3.4. Dissolution behavior of glasses before and after CCC treatment

Fig. 6 presents the normalized loss (NL) curves for selective parent (glasses) and CCC-treated (glass or glass-ceramic) samples, while the NL curves for all the samples (before and after CCC) are presented in Figures S2 and S3. The elemental concentrations obtained from ICP-OES and the calculated NL values for all the elements of all the samples are presented in Tables S4 and S5. As evident, the dissolution behavior of the investigated samples exhibits a considerable dependence on the chemical compositions and thermal history. Barring a few exceptions, B, Li, and Na dissolve in significantly higher concentrations than Al and Si in most tests. This behavior of the investigated samples can be attributed to the formation of an alteration layer, rich in Si and Al.

Since all the PCT experiments were conducted using one vessel per glass, the possibility of error in normalized release values has been estimated by using principles of error propagation. The procedure has been described in detail in the **section S1** of the supplementary information. The ultimate percentage error (standard deviation) in normalized release has been found to be in the range of 11–12% relative to the

actual reported value. This indicates that although the estimated error is not negligible, the overall compositional trends obtained from the PCT experiments remain unchanged.

All the dissolution experiments have been monitored for their pH $_T$ $^\circ_C$. As shown in Fig. 7, the pH $_T$ $^\circ_C$ values of the solution are significantly higher than that of DI water. This is attributed to the ion exchange of Li and Na $^+$ vs. H $^+$ into the solution during dissolution. Furthermore, it is found that the higher the NL values among different samples, the more significant is the increase in pH $_T$ $^\circ_C$ of the solution, as evident from the pH $_T$ $^\circ_C$ of AB-1 CCC. The significant impact of pH on the mechanism and kinetics of dissolution of borosilicate glasses is well reported in the literature [60, 76, 77]. Even one-unit in pH can result in up to one order of magnitude increase in the normalized dissolution rates [78–80]. This makes it difficult to directly compare the dissolution kinetics of different samples when pH of the solution is significantly evolving with the glass composition. Therefore, to evaluate the impact of composition and CCC treatment on the normalized dissolution rates, all dissolution rates were adjusted to a pH of 9.0 using Eq. (8) [79, 81].

$$log_{10}r_F = log_{10}r_I + \eta(9 - pH_{T \cdot C})$$
(8)

In Eq. (8), r_F is the pH-adjusted dissolution rate in $g/(m^2 \, day)$, r_I is the unadjusted rate in $g/(m^2 \, day)$, η is the pH power-law coefficient, and pH_T $^{\circ}$ C is the measured pH of the test solution. We have assumed a value of 0.40 for η as a typical value for the power-law coefficient according to the literature [82]. For the 28-d rate, the pH_T $^{\circ}$ C value was chosen as the average measured pH value between 1 – 28 days, while the pH_T value

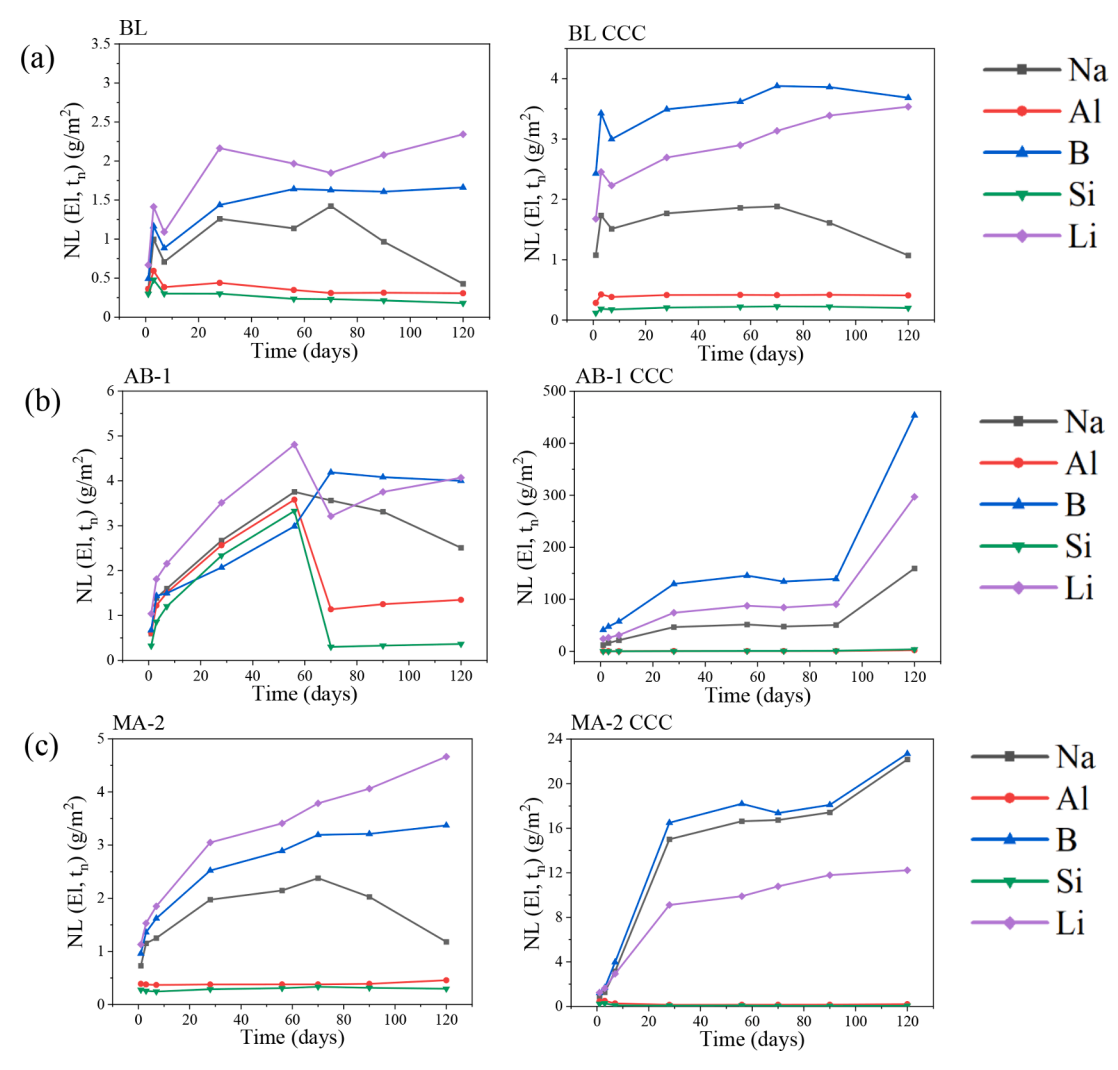
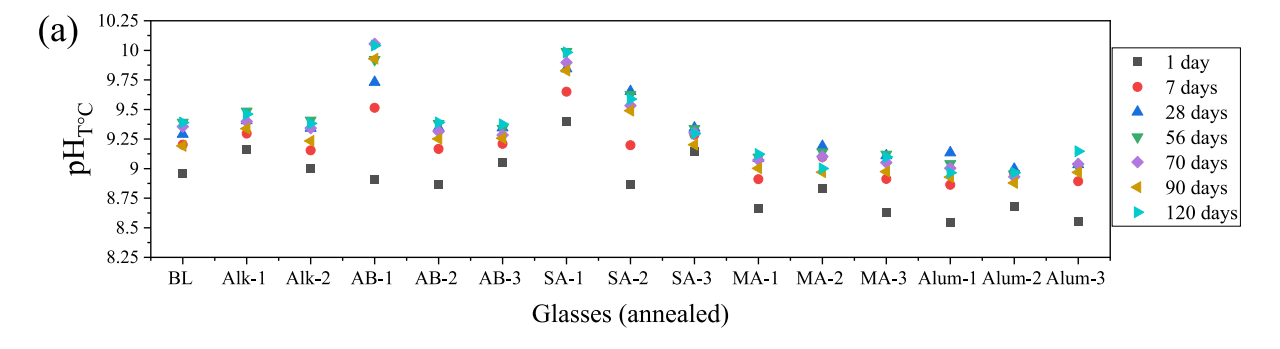


Fig. 6. Normalized loss (NL (El, t_n)) vs. time curves of (a) BL, (b) AB-1 and (c) MA-2 parent glasses and CCC treated samples.



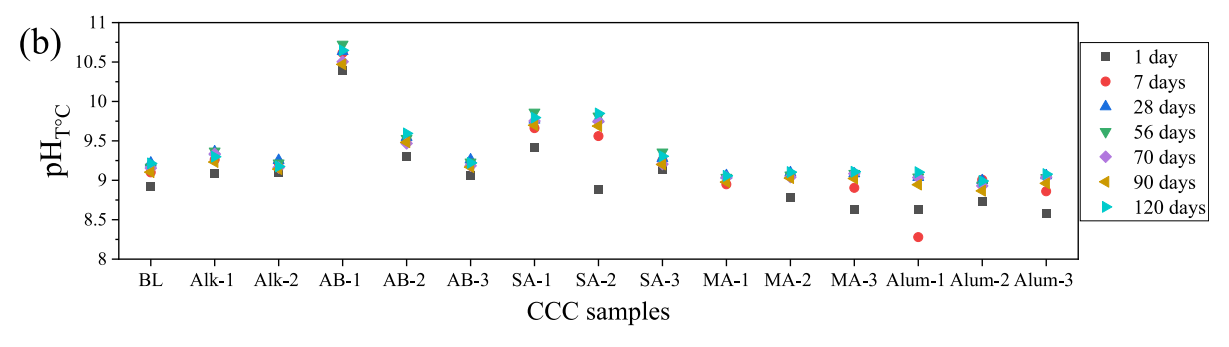


Fig. 7. pH of solutions during the corrosion of (a) parent glasses and (b) CCC-treated samples over the period of 120 days.

chosen for the long-term rate was the average pH value between 28 – 90 days.

Both the composition and CCC treatments had an impact on the dissolution of glasses and resulting glass-ceramics. To obtain a comprehensive understanding of dissolution behavior, this section has been divided into the following two sub-sections: (1) Impact of composition, and (2) Impact of CCC treatment, on the dissolution behavior of glasses.

3.4.1. Impact of composition on the dissolution behavior of glasses

Table 7 presents the normalized release of boron (NL_B) (g/m^2) from all the parent glasses after 7 and 120 days. Further, Table 8 presents the 28-d and longer-term pH-adjusted dissolution rates calculated from the normalized release concentrations of lithium in these experiments. The unadjusted 28-d and longer-term dissolution rates are presented in Table S6. Among the samples, the trends in 7-day PCT-B NL_B values

Table 7 7-day and 120-day PCT normalized loss (g/m²) of boron (NL_B) from the parent glasses and their respective CCC samples. (Average relative standard deviation is estimated to be $\pm 12\%$ of the actual value of the normalized loss).

	7-day PCT NL _B (g/m ²)		120-day PCT NL _B (g/m ²)		
	Parent glass	CCC samples	Parent glass	CCC samples	
BL	0.88	2.99	1.66	3.68	
Alk-1	2.31	2.66	4.68	4.88	
Alk-2	0.30	27.51	0.51	39.71	
MA-1	0.60	1.51	1.11	2.23	
MA-2	1.62	3.97	3.37	22.69	
MA-3	0.38	0.94	0.33	2.02	
Alum-1	0.62	0.67	5.86	1.46	
Alum-2	1.23	1.68	17.15	18.39	
Alum-3	0.55	0.67	2.30	1.88	
AB-1	1.50	57.52	4.00	453.65	
AB-2	0.53	17.38	0.52	19.43	
AB-3	3.48	3.76	5.99	6.94	
SA-1	9.78	10.37	14.79	17.10	
SA-2	1.55	7.79	11.46	29.77	
SA-3	1.43	3.75	3.57	4.18	

Table 8 28-d and longer-term PCT pH-adjusted dissolution rates (\times 10⁻²) of lithium (g/ (day m²) (Average relative standard deviation is estimated to be 12% of the actual value of the normalized loss rate).

	B ₂ O ₃ :SiO ₂ ratio		28-d rate (1–28 days) (× 10^{-2} g/(day m ²))		Longer-term rate (28–90 days) ($\times 10^{-2}$ g/(day m ²))		
		Parent	CCC	Parent	CCC		
		glass	samples	glass	samples		
BL	0.506	4.73	3.11	0.61	0.98		
Alk-1	0.754	15.35	13.08	2.32	2.84		
Alk-2	0.319	2.28	81.78	0.30	3.05		
MA-1	0.506	2.85	16.98	0.83	0.53		
MA-2	0.754	6.33	29.97	1.53	4.13		
MA-3	0.319	2.76	3.51	0.30	0.46		
Alum-	0.506	8.37	4.74	1.97	0.69		
1							
Alum-	0.754	18.00	14.73	5.98	3.53		
2							
Alum-	0.319	6.12	3.63	1.30	0.96		
3							
AB-1	0.222	12.06	45.76	0.80	6.00		
AB-2	0.364	1.61	46.55	0.43	2.03		
AB-3	0.647	11.61	10.45	2.44	3.65		
SA-1	0.642	24.72	24.82	1.42	1.67		
SA-2	0.589	10.21	23.32	3.19	6.95		
SA-3	0.443	4.97	33.97	1.29	1.44		

(Table 7) mostly correlate well with those in 28-d dissolution rates – samples which show a high 7-day $\rm NL_B$ value also have a high lithium 28-d dissolution rate.

The baseline parent glass, BL, shows an NL_B of $0.88 \ g/m^2$ after 7 days and a 28-d dissolution rate of $4.73 \times 10^{-2} \ g/m^2/d$. The values of NL_B (Table 7) and dissolution rates (Table 8) indicate that increasing B₂O₃: SiO₂ ratio leads to an increase in the normalized release rates of B, Na, and Li from glasses irrespective of whether the glass compositions belong in the peralkaline (BL, Alk-1 and Alk-2), metaluminous (MA-1, MA-2, and MA-3) or peraluminous regime (Alum-1, Alum-2, and Alum-3). This trend of decreasing durability with increasing B₂O₃:SiO₂ ratio

can be explained by the gradual substitution of Si–O–T linkages by B–O–T (T=B, Si, Al) linkages in the glass structure. The B–O–T linkages are known to exhibit lower resistance towards hydrolysis compared to Si–O–Si and Si–O–Al linkages [37, 83-85].

The effect of changing the (Li+Na):Al ratio can be observed by comparing the performance of BL glass with that of MA-1 and Alum-1 glasses. The metaluminous glass, MA-1, shows a lower 7-day NL_B value and a lower 28-d dissolution rate (for Li) when compared to the peralkaline glass, BL. This trend is also followed in the 120-day NL_B and the longer-term dissolution rates (for Li), suggesting that moving from peralkaline to a metaluminous regime leads to an improvement in the chemical durability of alkali aluminoborosilicate glasses. The higher chemical durability of glass MA-1 in comparison to the glass BL can be explained based on its higher degree of polymerization, as the majority of Na^+ and Li^+ in the structure of glass MA-1 are expected to charge compensate AlO_4^- units, thus, resulting in minimal fraction of NBOs in the glass structure. This explanation is well supported by the ^{11}B and ^{27}Al MAS NMR spectra of glass MA-1 (Fig. 2).

With further decrease in (Li+Na):Al ratio to <1, Alum-1 shows a 7day NL_B value of 0.62 g/m², i.e., smaller than BL but comparable to MA-1. However, its 120-d NL_B is significantly higher (5.86 g/m²) than BL (1.66 g/m^2) and MA-1 (1.11 g/m^2) glasses. In terms of the dissolution rates of Li, the glass Alum-1 shows a significantly higher 28-d dissolution rate, i.e., 8.37×10^{-2} g/(m² day) as compared to that of glass BL, i.e., 4.73×10^{-2} g/(m² day). Similar trends can be observed when comparing the dissolution kinetics of glasses Alk-1, MA-2 and Alum-2, or Alk-2, MA-3, Alum-3. Thus, it can be generalized that the chemical durability of glasses in the present work increases in the order: metaluminous > peralkaline > peraluminous. These results are intriguing as, theoretically, peraluminous glasses are expected to exhibit either comparable or superior chemical durability than their peralkaline analogues owing to higher degree of polymerization in their glass network [86]. One possible reason for faster kinetics of dissolution of Alum-1 glass can be the formation of non-negligible fraction of AlO5 units in its glass structure, as shown in Fig. 3 and Table 5. However, a detailed investigation into the impact/role of five-coordinated aluminum on the

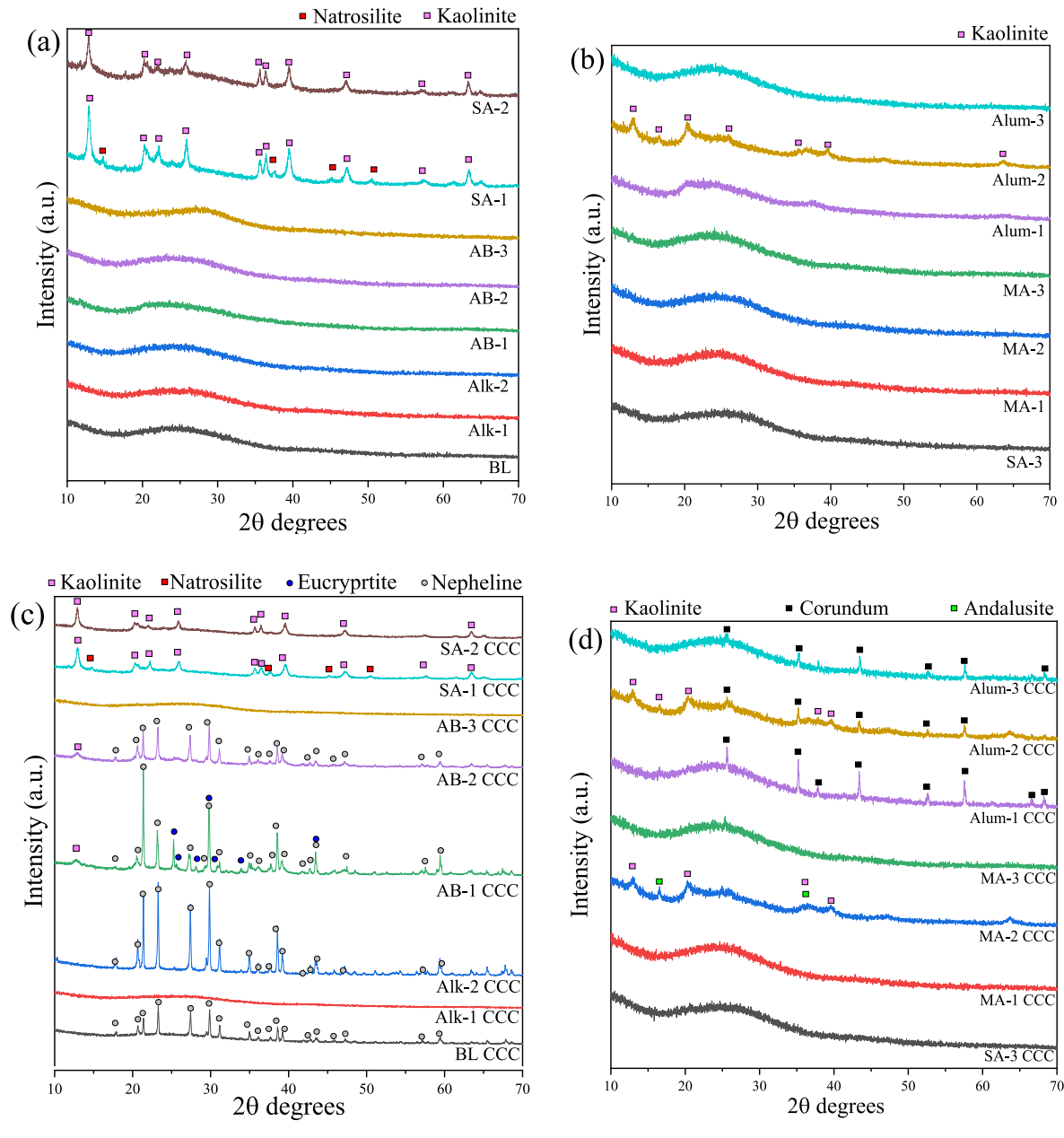


Fig. 8. X-ray diffractograms of post-dissolution powders of parent glasses (a and b) and CCC-treated samples (c and d).

dissolution behavior of alkali aluminoborosilicate glasses needs to be performed to unearth the exact reason. Also, these trends may explain the non-linear impacts of Al_2O_3 on short-term dissolution reported by Vienna and Crum [87].

As compared to the baseline glass, BL, decreasing the B_2O_3 : Al_2O_3 ratio leads to some interesting results in the PCT responses of these glasses. A decrease in the B_2O_3 : Al_2O_3 ratio from BL to AB-2 leads to a decrease in the 7-day NL_B value to 0.53 g/m² in AB-2. However, a further decrease in B/Al in AB-1 leads to a significant increase in the 7-day NL_B value to 1.50 g/m². These results again complement the trends reported above, i.e., peraluminous glasses exhibit higher dissolution kinetics than their peralkaline or metaluminous counterparts. On the other hand, increasing the B_2O_3 : Al_2O_3 ratio from BL to AB-3 glass results in an increase in the NL of B, Li, and Na. This suggests that excessive boron concentration in the glass has an adverse impact on the PCT performance of these aluminoborosilicate glasses. The convoluted non-

linear impacts of boron and aluminum were empirically shown previously, and we can now begin to see the structural reasons [87]. Furthermore, varying the $\rm Al_2O_3:SiO_2$ ratio of glasses shows that a reduction in SiO_2-content increases the 7-day NL_B value as denoted by the normalized release concentrations of 9.78 g/m² of SA-1, 1.55 g/m² in SA-2, and 1.43 g/m² in SA-3 glasses. These trends can be attributed to the weakening of the glass network due to decreasing SiO_2 content.

Fig. 8 presents the XRD results of samples obtained at the end of the dissolution experiments. Among all the glasses, only SA-1, SA-2, and Alum-2 are found to have precipitated crystalline phases, with kaolinite (Al $_2$ Si $_2$ O $_5$.4(OH); PDF #97–002–0593; triclinic) being the phase precipitated in all the three samples. Previous studies have shown that the kaolinite precipitates as a secondary phase during the dissolution of aluminosilicate glasses [88, 89]. Low-intensity peaks corresponding to natrosilite (Na $_2$ Si $_2$ O $_5$; PDF # 97–002–7762; monoclinic) were also detected in the SA-1 sample. Similarly, low-intensity peaks

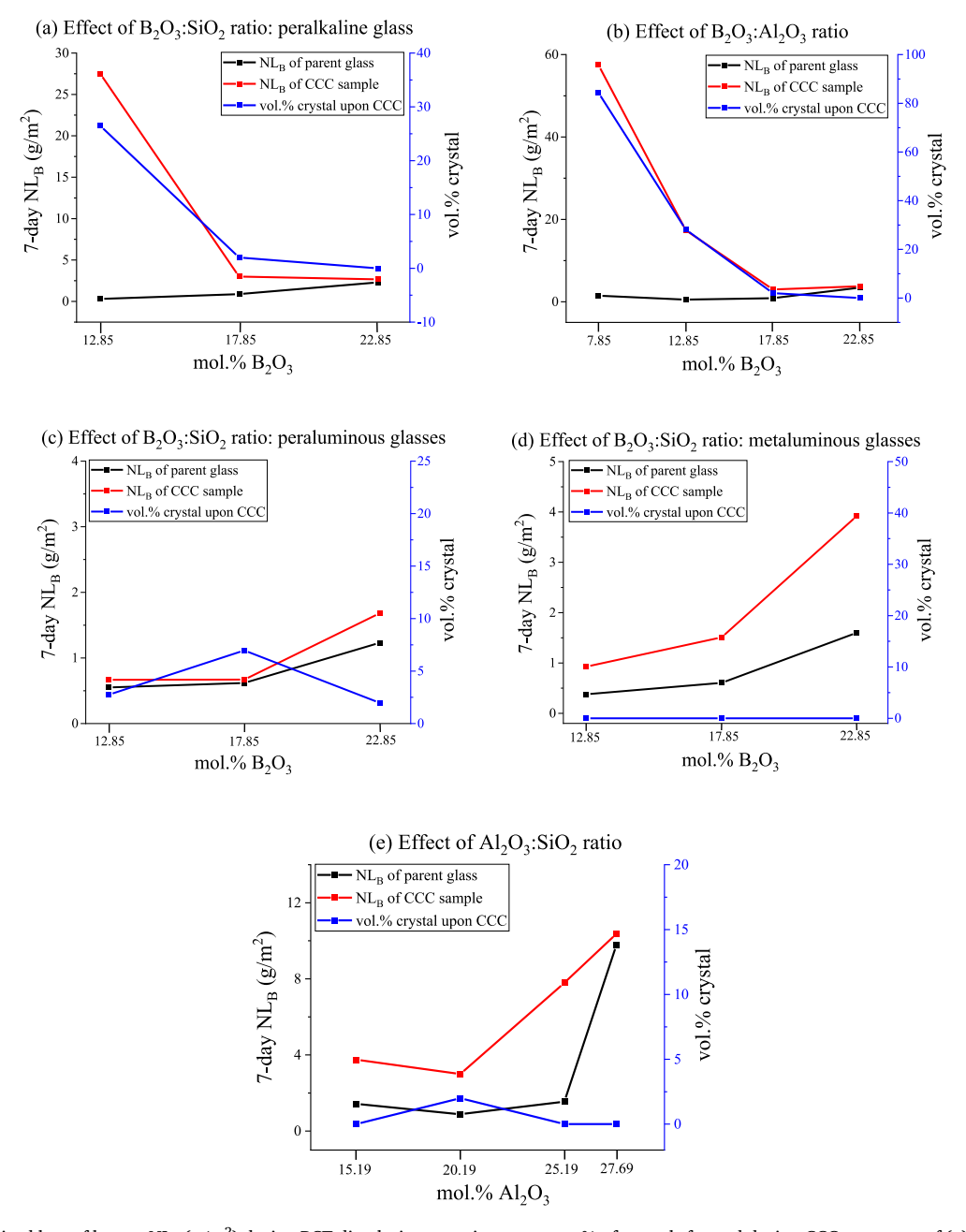


Fig. 9. 7-day normalized loss of boron, NL_B (g/m²) during PCT dissolution experiments vs. wt.% of crystals formed during CCC treatment of (a) BL, Alk-1 and Alk-2; (b) AB-x; (c) Alum-x; (d) MA-x; and (e) SA-x glasses.

corresponding to andalusite (Al₂SiO₅; PDF #97-017-2732; orthorhombic) and aluminum oxide (Al₂O₃; PDF # 97–015–1589; hexagonal) were detected in Alum-2 glass sample. Comparing the compositions of these three glasses with the rest of the glasses studied here, it is evident that SA-1, SA-2, and Alum-2 all have a relatively low SiO2 content, and a relatively high Al₂O₃ and B₂O₃ content. A lower SiO₂ content in the glass composition is likely to make the aluminoborosilicate network weaker than the baseline glass due to lower proportion of Si-O-Si linkages, eventually leading to the precipitation of aluminosilicate phases over 120 days. Furthermore, a comparison between normalized concentrations of B, Li and Na of SA-1, SA-2, and Alum-2 glasses with the rest of the glasses shows that a low-SiO2 content and corresponding formation of kaolinite correlates with an increase in a longer-term dissolution rate as shown in Table 8. The observation of precipitation of aluminosilicate phases accompanied with increased dissolution rate in case of low-SiO₂ samples can be compared with previous studies that show precipitation of zeolites associated with the resumption of dissolution, also known as Stage III dissolution [90-92]. In the present study, while the parent samples have shown precipitation of aluminosilicate phases such as kaolinite, we have not observed zeolitic phases and correspondingly have not observed a resumption of high rate of Stage III dissolution.

3.4.2. Impact of CCC treatment on dissolution behavior Tables 7 and 8 present normalized loss of boron NL_B (g/m²) values

and dissolution rates (g/(day m²)) of CCC-treated samples, respectively. Fig. 9 presents the 7-d NL_B (g/m²) from the CCC-treated samples as a function of glass chemistry, crystallization behavior and thermal history. Based on the observed trends, it can be concluded that the dissolution kinetics of the final waste form are controlled by the volume fraction of nepheline or similar alkali aluminosilicate phases that crystallize during the CCC-tests (see Figs. 9a and 9b). The crystallization of Al₂O₃ in CCC-tests has a minimal impact on the durability of the final waste form (see Fig. 9c). Finally, in the glasses that tend to stay amorphous after CCC tests, thermal history plays an essential role in dictating their dissolution kinetics. As evident from Figs. 9c, 9d and 9e, the CCCtreated glasses exhibit higher NLB values than their parent analogues. At first glance, it seems that these results tend to disagree with the previously reported literature on this subject where it has been shown that the borosilicate glasses with lower fictive temperatures exhibit slower dissolution kinetics [37, 38]. However, a closer look at the compositional make-up of the glasses studied here shows that these glasses may be considered as alkali-poor borosilicate glasses with R (alkali-to-boron ratio) < 0.5, as discussed in Section 3.3. Therefore, the structure of CCC-treated glasses, in this case, is expected to exhibit a higher fraction of Si-O-B^[3], B-O-B and Si-O-Si bonds instead of a homogeneous mixed silicate-borate network. Thus, the formation of higher fraction of bonds that are easy to hydrolyze, for example, Si-O-B^[3] and B-O-B [84], may be attributed to the higher dissolution kinetics of these glasses than their

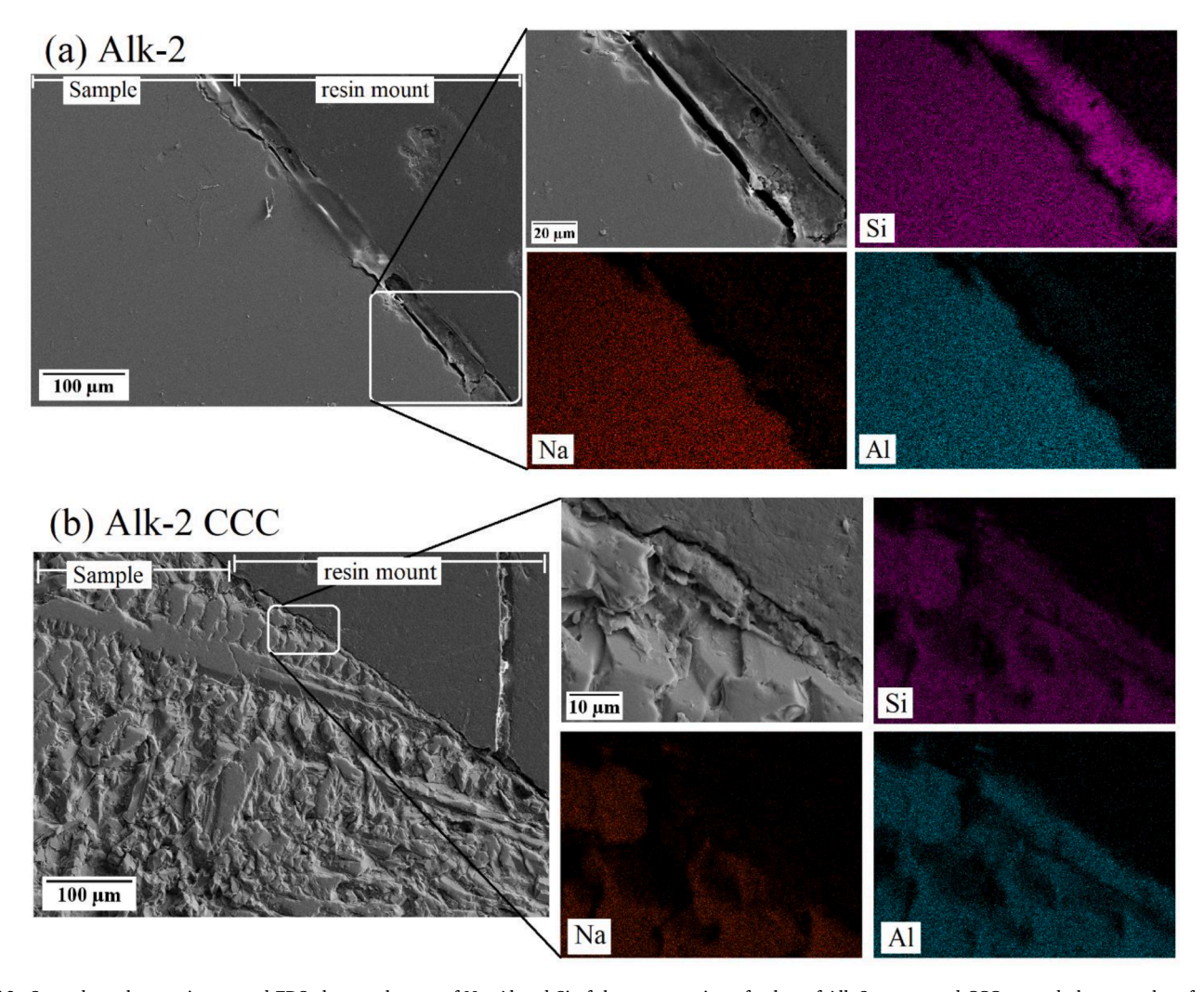


Fig. 10. Secondary electron image and EDS elemental maps of Na, Al and Si of the cross-section of cubes of Alk-2 parent and CCC-treated glass samples after the completion of PCT experiment. The image focuses on edge of the cube denoting interface between cube and the mounting resin.

parent analogues.

It is noteworthy that most parent and CCC samples studied here do not show a significant acceleration in alteration rate that characterizes Stage III behavior after 120 d. However, in the case of the AB-1 CCC sample, there is a significant increase in the normalized release from 90-days to 120 days, which may signify a transition to Stage III. This sample has high fractions of nepheline and eucryptite in its bulk glass-ceramic and precipitated kaolinite phase.

SEM-EDS analysis was conducted on cross-sections of the cubes obtained after the end of dissolution experiments. Figs. 10a and 10b present SEM micrograph along with its Si, Al, and Na EDS elemental maps of Alk-2 (parent glass) and CCC samples, respectively, focused on the edge of the cube. It can be observed from the EDS elemental maps that the alteration layer is rich in Si in case of the glass and deficient in both Al and Na. On the other hand, the CCC sample has an alteration layer rich in both Si and Al. The SEM image also shows the rough morphology in its bulk region that is characteristic of nepheline crystals (Fig. 10b). This is followed by a valley-like region in some areas along the edge of the sample, while other samples show the presence of the Sirich layer within that valley. The absence of Si-rich deposits and the formation of a valley in these regions of the samples is likely a result of

sample preparation, which could have led to the removal of some parts of the alteration layer. The thickness of this alteration layer varies from 5 to 15 μm between different samples.

Fig. 11 shows a comparison of elemental mapping obtained from the energy dispersive spectroscopy conducted on cubes of the MA-2 glass (Fig. 11a) and corresponding CCC sample (Fig. 11b) obtained at the end of the 120-day dissolution experiments. As mentioned before, silicone RTV adhesive was applied to certain areas of the cubes so that those areas would remain unaffected by chemical dissolution. Thus, these images show surfaces with altered as well as unaltered regions. The glass sample cube does not show any significant difference between the altered and unaltered surfaces except for pits and cracks which are likely a result of the release of B, Li, and Na elements from this glass. The CCC counterpart of MA-2 on the other hand, shows large crystals with cracks and voids in the altered surface of the cube which is indicative of the greater extent of dissolution as compared to the parent glass and also a likely result of the precipitation of kaolinite during the PCT experiment. These significant differences in the surface microstructure of samples suggest a change in the kinetics of dissolution.

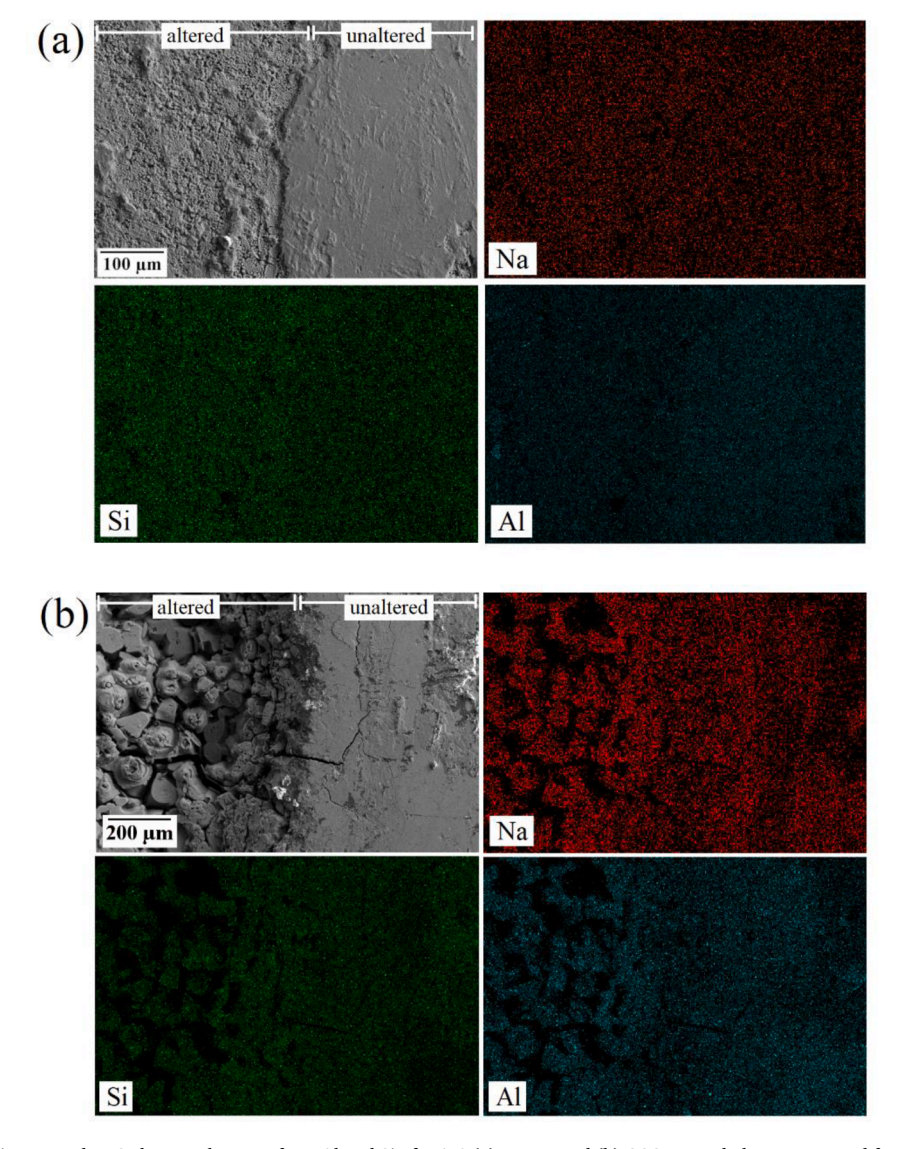


Fig. 11. Secondary electron image and EDS elemental maps of Na, Al and Si of MA-2 (a) parent and (b) CCC-treated glasses captured from the top surface of the cubes after the completion of PCT experiment. The images focus on the boundary between altered surface and unaltered surface of the cubes.

4. Conclusions

In this study, the compositional dependence of crystallization and chemical durability in mixed alkali aluminoborosilicate glasses has been studied over a broad composition space covering peralkaline, metaluminous and peraluminous regions of the glass forming system. The glasses have been subjected to CCC treatment, and their chemical durability has been investigated (before and after CCC tests) using PCT-B over a period of 120 days. The overarching goal is to aid in the development of nuclear waste glass compositions with enhanced waste loadings without compromising with their long-term performance. The following are the key conclusions of this study:

- (i) In peralkaline regime, increasing the B₂O₃:SiO₂ ratio is beneficial in suppressing nepheline crystallization during CCC. However, significantly high concentration of B₂O₃ can be detrimental for the durability of the final waste form. Therefore, a balance needs to be maintained wherein glasses with minimal tendency towards devitrification and suitable chemical durability can be designed.
- (ii) In metaluminous and peraluminous glasses, the variation of B_2O_3 : SiO_2 ratio did not have a significant impact on the propensity of nepheline formation during CCC. While corundum tends to precipitate in peraluminous glasses as the crystalline phase during CCC tests, it exhibits a minimal impact on the overall durability of the final waste form.
- (iii) Among all the factors studied in this work, i.e., glass composition (and structure), crystallization and thermal history, the crystallization of nepheline has the most dominant impact on the durability of the glassy waste form.
- (iv) The durability of the parent glasses investigated in the present study can be generalized by the following trend: metaluminous > peralkaline > peraluminous. The low durability of peraluminous glasses is intriguing and warrants further investigation.
- (v) The thermal history has been shown to exhibit a significant impact on the durability of the glassy waste form. Interestingly, the glasses with low fictive temperature, i.e., CCC-tested, exhibit faster dissolution kinetics compared to the parent glasses with higher fictive temperatures.
- (vi) The glasses in metaluminous and peraluminous regions with low SiO₂ content are prone to the precipitation of crystalline phases, e.g., kaolinite, during the long-term dissolution.
- (vii) Finally, the results highlight the need to strengthen the nepheline predictive models with more data and emphasize development of more quantitative structure – property based predictive models.

Declaration of Competing Interest

The authors declare that they have no known competing financial interests or personal relationships that could have appeared to influence the work reported in this paper.

Acknowledgement

This material is based upon work supported by the US Department of Energy (DOE), Office of River Protection, Waste Treatment & Immobilization Plant (WTP), through contract number 89304018CEM000006, and National Science Foundation under Grant No. 2034871. The authors are thankful to Dr. Nicholas Stone-Weiss (Corning Incorporated) and Dr. Jim Neeway (PNNL) for their suggestions/discussion. The authors would like to thank Dr. Albert Kruger (US Department of Energy) for the technical oversight of the work.

Supplementary materials

Supplementary material associated with this article can be found, in the online version, at doi:10.1016/j.jnoncrysol.2022.121694.

References

- A.A. Kruger, Advances in Glass Formulations for Hanford High-Aluminum, High-Iron and Enhanced Sulphate Management in HLW Streams –13000. No. ORP-54302-FP Rev O. Hanford Site (HNF), Richland, WA (United States), 2013.
- [2] J.D. Vienna, Nuclear waste vitrification in the United States: recent developments and future options, Int. J. Appl. Glass Sci. 1 (2010) 309–321.
- [3] J.D. Vienna, J.O. Kroll, P.R. Hrma, J.B. Lang, J.V. Crum, Submixture model to predict nepheline precipitation in waste glasses, Int. J. Appl. Glass Sci. 8 (2017) 143–157.
- [4] R.A. Peterson, E.C. Buck, J. Chun, R.C. Daniel, D.L. Herting, E.S. Ilton, G. J. Lumetta, S.B. Clark, Review of the scientific understanding of radioactive waste at the US DOE Hanford site, Environ. Sci. Technol. 52 (2) (2018) 381–396.
- [5] A. Goel, J.S. McCloy, K.M. Fox, C.J. Leslie, B.J. Riley, C.P. Rodriguez, M. J. Schweiger, Structural analysis of some sodium and alumina rich high-level nuclear waste glasses, J Non Cryst Solids 358 (2012) 674–679.
- [6] J. McCloy, N. Washton, P. Gassman, J. Marcial, J. Weaver, R. Kukkadapu, Nepheline crystallization in boron-rich alumino-silicate glasses as investigated by multi-nuclear NMR, Raman, & Mossbauer spectroscopies, J. Non Cryst. Solids 409 (2015) 149–165.
- [7] Hanford Tank Waste retrieval, treatment, and Disposition Framework, U.S. DOE, Washington D.G. 2013.
- [8] X. Guo, S. Gin, P. Lei, T. Yao, H. Liu, D.K. Schreiber, D. Ngo, G. Viswanathan, T. Li, S.H. Kim, J.D. Vienna, J.V. Ryan, J. Du, J. Lian, G.S. Frankel, Self-accelerated corrosion of nuclear waste forms at material interfaces, Nat. Mater. 19 (2020) 310–316.
- [9] H. Li, J. Vienna, P. Hrma, D. Smith, M. Schweiger, Nepheline precipitation in highlevel waste glasses: compositional effects and impact on the waste form acceptability, MRS Online Proc. Library Archive 465 (1996) 261–268.
- [10] H. Li, J.D. Vienna, P. Hrma, D.E. Smith, M.J. Schweiger, Nepheline precipitation in high-level waste glasses: compositional effects and impact on the waste form acceptability, MRS Online Proc. Library 465 (1) (1996) 261–268.
- [11] D.S. Kim, D.K. Peeler, P. Hrma, Effect of crystallization on the chemical durability of simulated nuclear waste glasses, Ceram. Trans. 61 (1995) 177–185.
- [12] D.L. McClane, J.W. Amoroso, K.M. Fox, M.C. Hsieh, M.R. Kesterson, A.A. Kruger, Nepheline crystallization and the residual glass composition: understanding waste glass durability, Int. J. Appl. Glass Sci. 11 (4) (2020) 649–659.
- [13] A. Deshkar, J. Marcial, S.A. Southern, L. Kobera, D.L. Bryce, J.S. McCloy, A. Goel, Understanding the structural origin of crystalline phase transformations in nepheline (NaAlSiO₄) based glass-ceramics, J. Am. Ceram. Soc. 100 (2017) 2859–2878.
- [14] A. Deshkar, M. Ahmadzadeh, A. Scrimshire, E. Han, P.A. Bingham, D. Guillen, J. McCloy, A. Goel, Crystallization behavior of iron-and boron-containing nepheline (Na₂O• Al₂O₃• 2SiO₂) based model high-level nuclear waste glasses, J. Am. Ceram. Soc. 102 (2019) 1101–1121.
- [15] A. Deshkar, O. Gulbiten, R.E. Youngman, J.C. Mauro, A. Goel, Why does B₂O₃ suppress nepheline (NaAlSiO₄) crystallization in sodium aluminosilicate glasses? Phys. Chem. Chem. Phys. 22 (2020) 8679–8698.
- [16] H. Li, P. Hrma, J.D. Vienna, M. Qian, Y. Su, D.E. Smith, Effects of Al₂O₃, B₂O₃, Na₂O, and SiO₂ on nepheline formation in borosilicate glasses: chemical and physical correlations, J. Non-Cryst. Solids 331 (2003) 202–216.
- [17] J. Marcial, J. Crum, O. Neill, J. McCloy, Nepheline structural and chemical dependence on melt composition, Am. Mineral. 101 (2016) 266–276.
- [18] J. Marcial, J. Kabel, M. Saleh, N. Washton, Y. Shaharyar, A. Goel, J.S. McCloy, Structural dependence of crystallization in glasses along the nepheline (NaAlSiO₄) eucryptite (LiAlSiO₄) join, J. Am. Ceram. Soc. 101 (2018) 2840–2855.
- [19] J. Marcial, M. Saleh, D. Watson, S.W. Martin, C.L. Crawford, J.S. McCloy, Boron-speciation and aluminosilicate crystallization in alkali boroaluminosilicate glasses along the NaAl_{1-x}B_xSiO₄ and LiAl_{1-x}B_xSiO₄ joins, J Non Cryst Solids 506 (2019) 58_67
- [20] Y. Shaharyar, J.Y. Cheng, E. Han, A. Maron, J. Weaver, J. Marcial, J.S. McCloy, A. Goel, Elucidating the effect of iron speciation (Fe²⁺/Fe³⁺) on crystallization kinetics of sodium aluminosilicate glasses, J. Am. Ceram. Soc. 99 (2016) 2306–2315.
- [21] S.A. Utlak, T.M. Besmann, Thermodynamic assessment of the pseudoternary Na₂O-Al₂O₃-SiO₂ system, J. Am. Ceram. Soc. 101 (2018) 928–948.
- [22] S.A. Utlak, T.M. Besmann, Thermodynamic assessment of the Na₂O-Al₂O₃-SiO₂-B₂O₃ pseudo-binary and-ternary systems, J. Chem. Thermodyn. 130 (2019)
- [23] A. Krishnamurthy, V.K. Michaelis, S. Kroeker, Network formation in borosilicate glasses with aluminum or gallium: implications for nepheline crystallization, J. Phys. Chem. C 125 (2021) 8815–8824.
- [24] J.S. McCloy, M.J. Schweiger, C.P. Rodriguez, J.D. Vienna, Nepheline crystallization in nuclear waste glasses: progress toward acceptance of high-alumina formulations, Int. J. Appl. Glass Sci. 2 (2011) 201–214.
- [25] I. Sargin, C.E. Lonergan, J.D. Vienna, J.S. McCloy, S.P. Beckman, A data-driven approach for predicting nepheline crystallization in high-level waste glasses, J. Am. Ceram. Soc. 103 (2020) 4913–4924.
- [26] K.M. Fox, J.D. Newell, T.B. Edwards, D.R. Best, I.A. Reamer, R.J. Workman, Refinement of the Nepheline discriminator: Results of a Phase I study (WSRC-STI-00659), Savannah River National Laboratory, Aiken, SC, 2007.
- [27] K.M. Fox, T.B. Edwards, D.K. Peeler, Control of nepheline crystallization in nuclear waste glass, Int. J. Appl. Ceram. Technol. 5 (2008) 666–673.
- [28] K. Fox, J.J. Newell, T. Edwards, D. Best, I.I. Reamer, P.P. Workman, Refinement of the Nepheline Discriminator: Results of a Phase I Study, in, SRS (US), Funding

- organisation: US Department of Energy (United States), 2008, doi: 10.2172/924154.
- [29] X. Lu, I. Sargin, J.D. Vienna, Predicting nepheline precipitation in waste glasses using ternary submixture model and machine learning, J. Am. Ceram. Soc. 104 (2021) 5636–5647.
- [30] B.A. Stanfill, G.F. Piepel, J.D. Vienna, S.K. Cooley, Nonlinear logistic regression mixture experiment modeling for binary data using dimensionally reduced components, Qual. Reliab. Eng. Int. 36 (2020) 33–49.
- [31] A. Goel, J.S. McCloy, R. Pokorny, A.A. Kruger, Challenges with vitrification of Hanford High-Level Waste (HLW) to borosilicate glass – an overview, J. Non-Cryst. Solids: X 4 (2019), 100033.
- [32] P.K. Gupta, M.L. Lur, P.J. Bray, Boron coordination in rapidly cooled and in annealed aluminum borosilicate glass fibers, J. Am. Ceram. Soc. 68 (1985) C–82.
- [33] J. Wu, J.F. Stebbins, Quench rate and temperature effects on boron coordination in aluminoborosilicate melts, J. Non-Cryst. Solids 356 (2010) 2097–2108.
- [34] F. Angeli, O. Villain, S. Schuller, T. Charpentier, D. de Ligny, L. Bressel, L. Wondraczek, Effect of temperature and thermal history on borosilicate glass structure, Phys. Rev. B 85 (2012), 054110.
- [35] D. Möncke, G. Tricot, A. Winterstein-Beckmann, L. Wondraczek, E.I. Kamitsos, On the connectivity of borate tetrahedra in borate and borosilicate glasses, Phys. Chem. Glasses-Eur. J. Glass Sci. Technol. Part B 56 (2015) 203–211.
- [36] D. Moncke, D. Ehrt, H. Eckert, V. Mertens, Influence of melting and annealing conditions on the structure of borosilicate glasses, Phys. Chem. Glasses 44 (2003) 113–116.
- [37] N. Stone-Weiss, E.M. Pierce, R.E. Youngman, O. Gulbiten, N.J. Smith, J. Du, A. Goel, Understanding the structural drivers governing glass–water interactions in borosilicate based model bioactive glasses, Acta Biomater. 65 (2018) 436–449.
- [38] F. Angeli, T. Charpentier, P. Jollivet, D. de Ligny, M. Bergler, A. Veber, S. Gin, H. Li, Effect of thermally induced structural disorder on the chemical durability of International Simple Glass, npj Materials Degrad. 2 (2018) 31.
- [39] J. Kroll, J. Vienna, M.J. Schweiger, G. Piepel, S. Cooley, Results from Phase 1, 2, and 3 Studies On Nepheline Formation in High-Level Waste Glasses Containing High Concentrations of alumina, No. PNNL-26057 Rev 0.0, Pacific Northwest National Lab.(PNNL), Richland, WA (United States), 2016.
- [40] J.S. McCloy, C. Rodriguez, C. Windisch, C. Leslie, M.J. Schweiger, B.R. Riley, J. D. Vienna, Alkali/alkaline-earth content effects on properties of high-alumina nuclear waste glasses. Advances in Materials Science for Environmental and Nuclear Technology, John Wiley & Sons, Inc., 2010, pp. 63–76.
- [41] C.M. Jantzen, D.F. Bickford, Leaching of devitrified glass containing simulated SRP Nuclear Waste, MRS Proc. (1984) 44.
- [42] P. Lu, Y. Zan, J. Ren, T. Zhao, K. Xu, A. Goel, Structure and crystallization behavior of phosphorus-containing nepheline (NaAlSiO₄) based sodium aluminosilicate glasses, J. Non-Cryst. Solids 560 (2021), 120719.
- [43] P. Lu, S. Kapoor, L. Kobera, J. Brus, A. Goel, Structural dependence of crystallization in phosphorus-containing sodium aluminoborosilicate glasses, J. Am. Ceram. Soc. 105 (2022) 2556–2574.
- [44] L.S. Du, J.F. Stebbins, Network connectivity in aluminoborosilicate glasses: a high-resolution ¹¹B, ²⁷Al and ¹⁷O NMR study, J. Non-Cryst. Solids 351 (2005) 3508–3520.
- [45] J. Wu, J.F. Stebbins, Effects of cation field strength on the structure of aluminoborosilicate glasses: high-resolution ¹¹B, ²⁷Al and ²³Na MAS NMR, J. Non Cryst. Solids 355 (2009) 556–562.
- [46] J.T. Reiser, X. Lu, B. Parruzot, H. Liu, T. Subramani, H. Kaya, R.M. Kissinger, J. V. Crum, J.V. Ryan, A. Navrotsky, S.H. Kim, J.D. Vienna, Effects of Al:Si and (Al+Na):Si ratios on the properties of the International Simple Glass, Part I: Physical Properties, J. Am. Ceram. Soc. 104 (2021) 167–182.
- [47] X. Lu, J.T. Reiser, B. Parruzot, L. Deng, I.M. Gussev, J.C. Neuefeind, T.R. Graham, H. Liu, J.V. Ryan, S.H. Kim, N. Washton, M. Lang, J. Du, J.D. Vienna, Effects of Al: Si and (Al+Na):Si Ratios on the Properties of the International Simple Glass, Part II: Structure, J. Am. Ceram. Soc. 104 (2021) 183–207.
- [48] ASTM C 1285-14, Standard Test Methods For Determining Chemical Durability of Nuclear Hazardous, and Mixed Waste Glasses and Multiphase Glass Ceramics: The Product Consistency Test (PCT), West Conshohocken, PA, 2014.
- [49] L. Petkus, Canister centerline cooling data, revision 1, in: C. Musick (Ed.), River Protection Project, Waste Treatment Plant, Richland, WA, October 29, 2003.
- [50] J.D. Vienna, A. Fluegel, D.-.S. Kim, P.R. Hrma, Glass property data and models for estimating high-level waste glass volume (PNNL-18501), in Richland, WA (United States), 2009.
- [51] B. Parruzot, J. Ryan, J. George, R. Motkuri, J. Bonnett, L. Seymour, M. Derewiński, Multi-glass investigation of Stage III glass dissolution behavior from 22 to 90°C triggered by the addition of zeolite phases, J. Nucl. Mater. 523 (2019) 490–501.
- [52] D. Massiot, F. Fayon, M. Capron, I. King, S. Le Calvé, B. Alonso, J.O. Durand, B. Bujoli, Z. Gan, G. Hoatson, Modelling one-and two-dimensional solid-state NMR spectra, Magn. Reson. Chem. 40 (2002) 70–76.
- [53] D. Massiot, C. Bessada, J. Coutures, F. Taulelle, A quantitative study of 27Al MAS NMR in crystalline YAG, Journal of Magnetic Resonance (1969) 90 (1990) 231–242
- [54] X. Guo, M. Potuzak, J.C. Mauro, D.C. Allan, T.J. Kiczenski, Y. Yue, Unified approach for determining the enthalpic fictive temperature of glasses with arbitrary thermal history, J. Non-Cryst. Solids 357 (2011) 3230–3236.
- [55] Y.Z. Yue, J.D. Christiansen, S.L. Jensen, Determination of the fictive temperature for a hyperquenched glass, Chem. Phys. Lett. 357 (2002) 20–24.
- [56] C.T. Moynihan, A.J. Easteal, M.A. De Bolt, J. Tucker, Dependence of the fictive temperature of glass on cooling rate, J. Am. Ceram. Soc. 59 (1976) 12–16.

- [57] L.S. Du, J.F. Stebbins, Site preference and Si/B mixing in mixed-alkali borosilicate glasses: a high-resolution ¹¹B and ¹⁷O NMR study, Chem. Mater. 15 (2003) 3913–3921.
- [58] E.I. Morin, J. Wu, J.F. Stebbins, Modifier cation (Ba, Ca, La, Y) field strength effects on aluminum and boron coordination in aluminoborosilicate glasses: the roles of fictive temperature and boron content, Appl. Phys. A 116 (2014) 479–490.
- [59] H.R. Fernandes, S. Kapoor, Y. Patel, K. Ngai, K. Levin, Y. Germanov, L. Krishtopa, S. Kroeker, A. Goel, Composition-structure-property relationships in Li₂O-Al₂O₃-B₂O₃ glasses, J. Non-Cryst. Solids 502 (2018) 142–151.
- [60] N. Stone-Weiss, R.E. Youngman, R. Thorpe, N.J. Smith, E.M. Pierce, A. Goel, An insight into the corrosion of alkali aluminoborosilicate glasses in acidic environments, Phys. Chem. Chem. Phys. 22 (2020) 1881–1896.
- [61] B. Mysen, Aluminosilicate melts: structure, composition and temperature, Contrib. Mineral. Petrol. 127 (1997) 104–118.
- [62] E.V. Dubinsky, J.F. Stebbins, Quench rate and temperature effects on framework ordering in aluminosilicate melts, Am. Mineral. 91 (2006) 753–761.
- [63] D. Möncke, G. Tricot, A. Winterstein, D. Ehrt, E.I. Kamitsos, Preferential bonding in low alkali borosilicate glasses, Phys. Chem. Glasses-Eur. J. Glass Sci. Technol. Part B 58 (2017) 171–179.
- [64] L.S. Du, J.F. Stebbins, Nature of silicon-boron mixing in sodium borosilicate glasses: a high-resolution B-11 and O-17 NMR study, J. Phys. Chem. B 107 (2003) 10063–10076.
- [65] T.K. Bechgaard, A. Goel, R.E. Youngman, J.C. Mauro, S.J. Rzoska, M. Bockowski, L. R. Jensen, M.M. Smedskjaer, Structure and mechanical properties of compressed sodium aluminosilicate glasses: role of non-bridging oxygens, J. Non-Cryst. Solids 441 (2016) 49–57.
- [66] J. Wu, J.F. Stebbins, Temperature and modifier cation field strength effects on aluminoborosilicate glass network structure, J. Non-Cryst. Solids 362 (2013) 73, 81
- [67] K.M. Fox, D.K. Peeler, T.B. Edwards, Nepheline crystallization in nuclear waste glasses, Adv. Mater. Sci. Environ. Nuclear Technol. (2010).
- [68] C.P. Rodriguez, J.S. McCloy, M.J. Schweiger, J.V. Crum, A. Winschell. Optical basicity and nepheline crystallization in high alumina glasses (PNNL-20184), Pacific Northwest National Laboratory, Richland, WA, 2011 doi:10.2172/101921
- [69] S. Amma, J.W. Luo, S.H. Kim, C.G. Pantano, Effects of fictive temperature on the leaching of soda lime silica glass surfaces, J. Am. Ceram. Soc. 100 (2017) 1424 1421
- [70] T.J. Kiczenski, L.S. Du, J. Stebbins, The effect of fictive temperature on the structure of E-glass: A high resolution, multinuclear NMR study, J. Non-Cryst. Solids 351 (46–48) (2005) 3571–3578, https://doi.org/10.1016/j. inoncrysol.2005.09.026.
- [71] M.E. Lines, Can the minimum attenuation of fused silica be significantly reduced by small compositional variations? I. Alkali metal dopants, J. Non-Cryst. Solids 171 (1994) 209–218.
- [72] S. Kapoor, R.E. Youngman, K. Zakharchuk, A. Yaremchenko, N.J. Smith, A. Goel, Structural and chemical approach toward understanding the aqueous corrosion of sodium aluminoborate glasses, J. Phys. Chem. B 122 (2018) 10913–10927.
- [73] D. Möncke, D. Ehrt, H. Eckert, V. Mertens, Influence of melting and annealing conditions on the structure of borosilicate glasses, Phys. Chem. Glasses 44 (2003) 113–116.
- [74] D. Möncke, G. Tricot, D. Ehrt, E.I. Kamitsos, Connectivity of borate and silicate groups in a low-alkali borosilicate glass by vibrational and 2D NMR spectroscopy, J. Chem. Technol. Metallurgy (2015) 50.
- [75] J.R. Allwardt, B.T. Poe, J.F. Stebbins, The effect of fictive temperature on Al coordination in high-pressure (10GPa) sodium aluminosilicate glasses, Am. Mineral, 90 (2005) 1453–1457.
- [76] F. Wang, N. Balasubramanya, Q. Qin, R.E. Youngman, P. Mukherjee, N. Stone-Weiss, A. Goel, Multiscale investigation of the mechanisms controlling the corrosion of borosilicate glasses in hyper-alkaline media, J. Phys. Chem. C 124 (50) (2020) 27542–27557.
- [77] N. Stone-Weiss, N.J. Smith, R.E. Youngman, E.M. Pierce, A. Goel, Dissolution kinetics of a sodium borosilicate glass in Tris buffer solutions: impact of Tris concentration and acid (HCl/HNO₃) identity, Phys. Chem. Chem. Phys. 23 (2021) 16165–16179.
- [78] G. Perera, R.H. Doremus, Dissolution rates of commercial soda-lime and pyrex borosilicate glasses: influence of solution pH, J. Am. Ceram. Soc. 74 (1991) 1554–1558.
- [79] J.P. Icenhower, B.P. McGrail, W.J. Shaw, E.M. Pierce, P. Nachimuthu, D.K. Shuh, E. A. Rodriguez, J.L. Steele, Experimentally determined dissolution kinetics of Na-rich borosilicate glass at far from equilibrium conditions: implications for transition state theory, Geochim. Cosmochim. Acta 72 (2008) 2767–2788.
- [80] J.D. Vienna, J.J. Neeway, J.V. Ryan, S.N. Kerisit, Impacts of glass composition, pH, and temperature on glass forward dissolution rate, npj Mater. Degrad. 2 (2018) 22.
- [81] J. Hopf, S.N. Kerisit, F. Angeli, T. Charpentier, J.P. Icenhower, B.P. McGrail, C. F. Windisch, S.D. Burton, E.M. Pierce, Glass-water interaction: effect of high-valence cations on glass structure and chemical durability, Geochim. Cosmochim. Acta 181 (2016) 54–71.
- [82] J.J. Neeway, P.C. Rieke, B.P. Parruzot, J.V. Ryan, R.M. Asmussen, The dissolution behavior of borosilicate glasses in far-from equilibrium conditions, Geochim. Cosmochim. Acta 226 (2018) 132–148.
- [83] B.C. Bunker, G.W. Arnold, D.E. Day, P. Bray, The effect of molecular structure on borosilicate glass leaching, J. Non Cryst. Solids 87 (1986) 226–253.
- [84] S.K. Lee, C.B. Musgrave, P. Zhao, J.F. Stebbins, Topological disorder and reactivity of borosilicate glasses: quantum chemical calculations and ¹⁷O and ¹¹B NMR study, J. Phys. Chem. B 105 (2001) 12583–12595.

- [85] S. Gin, L. Neill, M. Fournier, P. Frugier, T. Ducasse, M. Tribet, A. Abdelouas, B. Parruzot, J. Neeway, N. Wall, The controversial role of inter-diffusion in glass alteration, Chem. Geol. 440 (2016) 115–123.
- [86] V. Piovesan, I. Bardez-Giboire, M. Fournier, P. Frugier, P. Jollivet, V. Montouillout, N. Pellerin, S. Gin, Chemical durability of peraluminous glasses for nuclear waste conditioning, npj Mater. Degrad. 2 (2018) 7.
- [87] J.D. Vienna, J.V. Crum, Non-linear effects of alumina concentration on Product Consistency Test response of waste glasses, J. Nucl. Mater. 511 (2018) 396–405.
- [88] P. Frugier, Y. Minet, N. Rajmohan, N. Godon, S. Gin, Modeling glass corrosion with GRAAL, npj Mater. Degrad. 2 (2018) 35.
- [89] G.S. Frankel, J.D. Vienna, J. Lian, J.R. Scully, S. Gin, J.V. Ryan, J. Wang, S.H. Kim, W. Windl, J. Du, A comparative review of the aqueous corrosion of glasses, crystalline ceramics, and metals, npj Mater. Degrad. 2 (2018) 15.
- [90] C.M. Jantzen, C.L. Trivelpiece, C.L. Crawford, J.M. Pareizs, J.B. Pickett, Accelerated leach testing of GLASS (ALTGLASS): I. Informatics approach to high level waste glass gel formation and aging, Int. J. Appl. Glass Sci. 8 (2017) 69–83.
- [91] W.L. Ebert, A.J. Bakel, N.R. Brown, Measurement of the glass dissolution rate in the presence of alteration phases, No. ANL/CMT/CP-88456; CONF-960804-40. Argonne National Lab (United States); Pacific Northwest National Lab (PNNL), Richland, WA (United States), 1996.
- [92] D.M. Strachan, T.L. Croak, Compositional effects on long-term dissolution of borosilicate glass, J. Non-Cryst. Solids 272 (2000) 22–33.